Kala, J., Andrys, J., Lyons, T.J., Foster, I.J. and Evans, B.J. (2015) Sensitivity of WRF to driving data and physics options on a seasonal time-scale for the southwest of Western Australia. Climate Dynamics, 44 (3-4). pp. 633-659.

Clim Dyn manuscript No.
(will be inserted by the editor)

Sensitivity of WRF to driving data and physics options on a seasonal time-scale for the southwest of Western Australia

Jatin Kala · Julia Andrys · Tom J. Lyons · Ian J. Foster · Bradley J. Evans

Received: date / Accepted: date

Abstract Regional climate models are sensitive to the forcing data used, as well as different model physics options. Additionally, the behaviour of physics parameterisations may vary depending on the location of the domain due to different climatic regimes. In this study, we carry out a sensitivity analysis of the Weather Research

Jatin Kala
Australian Research Council Centre of Excellence for Climate Systems Science and Climate Change Research Centre, University of New South Wales, Sydney, NSW, 2052, Australia
E-mail: J.Kala@unsw.edu.au

Tom J. Lyons and Julia Andrys
State Centre of Excellence for Climate Change Woodland and Forest Health, Murdoch University, Murdoch, WA, 6150, Australia

Ian J. Foster
Western Australian Department of Agriculture and Food, Bentley, WA, 6102, Australia

Bradley J. Evans
Department of Biological Sciences, Macquarie University, Macquarie Park, NSW, 2113, Australia

and Forecasting model to different driving data and model physics options over a 10-km resolution domain in the southwest of Western Australia, a region with Mediterranean climate. Simulations are carried out on a seasonal time-scale, in order to better inform future long-term regional climate simulations for this region. We show that the choice of radiation scheme had a strong influence on both temperature and precipitation; the choice of planetary boundary layer scheme has a particularly large influence on minimum temperatures; and, the choice of cumulus scheme or more complex micro-physics did not strongly influence precipitation simulations. More importantly, we show that the same radiation scheme, when used with different driving data, can lead to different results.

Keywords Dynamical downscaling · Physics parameterisation · Regional climate modeling · WRF

1 Introduction

The south-west of Western Australia (SWWA, see Fig. 1) is a region of significant agricultural production, with an estimated 13 million hectares of native vegetation cleared for agricultural land-use since the late 1820s (Huang et al, 1995; Andrich and Imberger, 2013). Grains are the main crops grown, with the commodity value of wheat, barley, and oats varying seasonally from approximately \$3,000 million to more than \$5,000 million between 2006 and 2010 (ABS, 2010). The region's crops are grown from winter to spring and rain-fed, and hence, crop yields are impacted heavily by inter-annual variations in temperature and precipitation. SWWA is also home to some of Australia's most iconic forests, which are sensitive to changes in temperature and precipitation (Hughes et al, 1993; Hughes, 2003; Evans and

Lyons, 2013). An understanding of the current climate of SWWA and how it might change in the future is therefore crucial for the planning and management of the region's agriculture and forestry sectors.

SWWA experiences a Mediterranean climate, with hot and dry summers, and cool and wet winters (Gentilli, 1971). Its climate is mainly driven by the position of the subtropical high pressure belt, which brings hot and dry continental air from the interior to the southwest during summer. Continental heating during summer results in surface heat troughs which control the penetration of sea-breezes and modulates temperature along the coast (Ma and Lyons, 2000; Ma et al, 2001). As the subtropical high pressure belt gradually moves northwards during winter and autumn, the region experiences most of its annual rainfall via the passage of frontal systems. Complex interactions between blocking-highs and frontal systems result in cut-off lows which are thought to account for up to 40% of the austral summer and spring rainfall (Pook et al, 2011) in central WA. Summer rainfall is also influenced by the passage of northwest cloud bands (Tapp and Barrell, 1984). Coastal regions are influenced by the presence of the Leeuwin Current, an anomalous western boundary current which drives warm tropical waters southwards (against prevailing winds) resulting in a moderation of winter temperatures and increased rainfall in the region relative to other western coastal margins (Reason et al, 1999). The main topographic influence on temperature and precipitation in SWWA is the Darling Scarp (Pitts and Lyons, 1989), which extends 200 km in a north-south direction from approximately 31°S to 34°S roughly 25 km from the coast, representing a sudden increase in topography of about 300 m from sea level (Fig. 1(c)). Previous studies have shown that a minimum horizontal resolution of 500 m is required to adequately simulate dynamical features of wind flow along the scarp (Pitts and Lyons, 1990). However, these simulations were restricted to a short time-scale of a few days, and did not explicitly focus on precipitation. Kala et al (2010) carried out longer simulations, focussing on two frontal events but at a lower resolution (20 km), and showed that whilst their model was able to capture the overall precipitation patterns, it was not able to accurately resolve orographically induced precipitation close to the coast due to a poor representation of the scarp.

In summary, there is considerable knowledge about the current climate of SWWA, however, there is limited information about current and future impacts at the regional scale. Regional climate models (RCMs) are a widely adopted tool to investigate current and future climatic changes at the regional scale. RCMs can dynamically downscale the synoptic fields from re-analysis products and/or global circulation models (GCMs), usually in the order of 100 to 250 km, to a finer resolution which is relevant at the farm/forest scale (1 to 10 km). An RCM which is being increasingly used for such purposes is the Weather Research and Forecasting (WRF) Advanced Research (WRF-ARW) modelling system (Skamarock et al, 2008). WRF has been used in regional climate simulations for the continental United States (Liang et al, 2005; Lo et al, 2008; Zhang et al, 2009; Leung and Qian, 2009; Bukovsky and Karoly, 2009; Caldwell et al, 2009; Salathe et al, 2010; Bukovsky and Karoly, 2011), East Asia (Kim and Song, 2010; Yuan et al, 2012), as well as Eastern Australia (Evans and McCabe, 2010), and is one of the RCMs being used for the Coordinated Regional climate Downscaling Experiment (CORDEX) (Giorgi et al, 2009) within the World Climate Research Program. WRF can be operated under a variety of configurations which can lead to varying results (e.g., Lo et al, 2008; Bukovsky and Karoly, 2009; Argüeso et al, 2011; Awan et al, 2011;

Evans et al, 2011), and hence it is crucial to test for the most appropriate model setup for a particular purpose over a given region/domain.

Different model versions and various settings of WRF were tested by Bukovsky and Karoly (2009) for the continental United States over a 4-month period. They generally recommend the use of Sea Surface Temperature (SST) updates, no inner nest feedback (i.e., no 2-way nesting), use of the NOAH land surface scheme (Ek et al, 2003) rather than the less complex 5-layer diffusion scheme, and the Kain-Fristch (KF) scheme (Kain, 2004) for convection. The effects of different WRF parameterisations were tested on a yearly time-scale for the European Alpine region (Awan et al, 2011), and it was found that parameterisations were sensitive to not just the region, but also the season. For example, cumulus and microphysics schemes have a stronger influence during summer months, while the PBL and radiation schemes have an influence throughout the year. This was related to the land-surface having a stronger influence as compared to large-scale synoptic fields, due to stronger surface heating during summer months. Overall, their best model performance was achieved by using the KF scheme for convection (cumulus parameterisation); the Yonsei University (YSU) scheme (Hong et al, 2006) for the PBL with the Monin-Obukhov (MO) scheme for the surface layer; and the Dudhia scheme (Dudhia, 1989) for radiation. Awan et al (2011) also reported their results to be region specific, namely, that WRF tends to over-predict precipitation in mountainous regions during both summer and winter months.

Argüeso et al (2011) investigated different WRF parameterisations for regional climate simulations over Southern Spain for a 10-year period. They determined that the cumulus and PBL schemes had a crucial impact on precipitation whereas the microphysics scheme had no noticeable impact. Minimum temperatures were sensitive to the choice of PBL scheme. Overall, they found that the combination of the Betts-Miller-Janjic (BMJ) cumulus scheme (Betts, 1986; Betts and Miller, 1986; Janjić, 1994, 2000) with the Asymmetric Convective Model (AC2) PBL scheme (Pleim, 2007a,b) and the WRF single moment 3-class microphysics scheme to perform the best. Flaounas et al (2011) and Crétat et al (2011) investigated the impacts of different convective and PBL schemes over Africa and found that the choice of PBL schemes have the strongest effect on temperature, and that precipitation variability was strongly influenced by the choice of convective parameterisation scheme. Evans et al (2011) carried out a 36-member WRF physics ensemble for storm events on the east coast of Australia. They found that whilst no particular combination of schemes performed best for all events, variables and metrics, the MYJ PBL scheme and BMJ cumulus schemes were robust in performance. They suggest that the YSU PBL scheme, KF scheme for convection, and RRTMG radiation scheme should not be used in combination for Eastern Australia. Evans et al (2011) also point out that the choice of physics scheme becomes more important as rainfall intensity increases.

Other than radiation, cumulus, and PBL schemes, the choice of land surface model (LSM) can strongly influence near surface temperature, moisture and winds. Jin et al (2010) investigated four LSMs in WRF and found that the more complex Community Land Model (CLMv3), generally outperformed the simper NOAH, RUC (Smirnova et al, 2000), and soil thermal diffusion scheme. They found no close relationship between the choice of LSM and precipitation. Prabha et al (2011) investigated the influence of NOAH and RUC LSMs on low-level jet dynamics and found that the RUC LSM performed better as compared to NOAH at lower elevations, but NOAH performed better at higher elevations. They also found that the

NOAH LSM resulted in higher vertical mixing as compared to RUC under stable conditions with low winds and high pressure. They however did not examine influences on precipitation. Mooney et al (2012) on the other hand, have shown that LSM choice not only influences temperature, but precipitation simulations, especially during the summer season over Europe. Namely, they showed that use of the NOAH LSM as compared to the RUC LSM, resulted in lower biases for temperature, but simulations using the RUC LSM generally had lower precipitation biases as compared to those using NOAH. Finally, a recent study by Stéfanon et al (2013) showed that use of the simple thermal diffusion scheme in WRF does not allow for the accurate simulation of heat-wave conditions over Europe, and more sophisticated LSMs such as the RUC, which explicitly resolve the treatment of soil processes is required.

Based on the current literature, it is clear that WRF is sensitive to the domain (location and boundaries), as well as different model parameterisations. Adequate testing of model configuration is therefore essential before carrying out long-term regional climate simulations. Accordingly, the aim of this paper is to test different model physics parameterisations and input data on simulated precipitation and temperature maxima and minima for SWWA. This forms the first part of a broader research project which aims at carrying out regional climate impact assessments for the agricultural and forestry sectors of SWWA. We note that the choice of model horizontal and vertical resolution can be equally important to the choice of boundary conditions and physics options. However, the resolution issue is not explicitly addressed in this paper, as model resolution for long term climate simulation is inherently limited to computational and storage constraints. This paper focuses on finding the best physics options and input forcing data, given these constraints. The next section describes the numerical experiments carried out, followed by a description of the observational data-sets and statistical analysis used.

2 Methods

2.1 Numerical Experiments

Yearly simulations were carried out with WRF-ARW Version 3.3 from October 2009 to November 2010, with the first two months being model spin-up and not used in the analysis. Two nested grids (1-way nesting) were used spanning 5150 km $\times$ 4200 km and 1760 km $\times$ 1440 km, at 50 km and 10 km resolutions respectively as shown in Figs. 1 (a) and (b). Both nested grids used 30 vertical levels, with levels more densely spaced within the PBL. Given the relatively long simulation period, use of nudging techniques was required to prevent model drift. This is commonly used for regional climate simulations (e.g., Argüeso et al, 2011) to ensure that the simulations retain the large scale features important in regional climate modeling. Based on previous studies which have investigated the influence of grid (analysis) versus spectral nudging techniques (Lo et al, 2008; Bowden et al, 2011; Liu et al, 2012; Omrani et al, 2013), we opted for spectral nudging applied to the outer domain (50 km) and above the PBL. Deep soil temperatures were set to a 150-day lagged averaging period and a series of sensitivity tests were carried out by changing the source of lateral boundary-conditions, SSTs, and the following model parameterisation schemes as outlined in Table 1; LSM, cumulus/convective, longwave and shortwave radiation, PBL, and cloud-microphysics.

The reference experiment (REF) was chosen because it follows the same configuration as in Evans and McCabe (2010) (except that Evans and McCabe (2010) used WRF3.0.1) which has shown adequate results for southeast Australia. REF uses 6-hourly boundary conditions from the 2.5 × 2.5 degree resolution National Centre for Atmospheric Research (NCAR) / National Centre for Environmental Prediction (NCEP) (commonly referred to as NNRP); the NOAH land surface model (LSM) (Chen and Dudhia, 2001a,b); the Rapid Radiative Transfer Model (RRTM) (Mlawer et al, 1997) and Dudhia schemes for long wave and shortwave radiation respectively; the KF scheme for convection; the YSU PBL scheme with MO surface layer scheme; surface skin temperatures within the NNRP data as SSTs; and the 5-class single moment microphysics scheme (WSM 5-Class).

Experiment N_SST is the same as REF, except that weekly mean SSTs from the National Oceanic and Atmospheric Administration (NOAA) SST product is used (Reynolds et al, 2002) and are interpolated to 6-hourly fields for use in WRF. The NOAA SST is at a 1.0 × 1.0 degree resolution and derived from satellites and in-situ measurements. On the other hand, NNRP data used in REF incorporate an earlier version of the same SST data-set (Reynolds and Smith, 1994), which are interpolated to daily values and used in the coupled ocean-atmosphere data assimilation system (Kalnay et al, 1996) to produce the NNRP product. When running WRF for the REF simulation, these SST data are not used directly, and the surface skin temperature output from NNRP is used instead, as the source of SST in WRF. Hence, the difference between experiments N_SST and REF is that N_SST uses a higher resolution SST in a direct fashion, whereas REF has a lower resolution, and indirectly incorporates satellite estimates of SST. This is illustrated in Fig. 2 for JJA (winter) and SON (spring) showing that NOAA SSTs are higher by up to 1.4°C close to the coast.

Experiments FNL and ERA are the same as REF, except that the 6-hourly boundary conditions are taken from the 1.0 × 1.0 degree NCEP Final (NCEP-FNL) Operational Global Data Assimilation System and the 1.5 × 1.5 degree ERA-interim (ERA-Int) re-analysis product (publicly available version) from the European Centre for Medium-Range Weather Forecasts (ECMWF) respectively. The NCEP-FNL data includes observations from the Global Telecommunications Systems and many other data sources, and is generated using the same model used by NCEP for their Global Forecast System (GFS). NCEP-FNL data are prepared after GFS is initialised such that the observational data can be used, but the product is only available from late 1999 to present. The ERA-Int data emanates from the ECMWF's ERA-40 product and involves better representations of the hydrological cycle, quality of the stratospheric circulation, handling of biases, and use of observations. The data are available from 1979 onwards and more detail can be found in Dee et al (2011). These experiments were carried out because, as to the author's knowledge, no previous study has explicitly compared these three re-analysis products in WRF. Additionally, these simulations will help better inform the influence of using data from different sources (e.g., different GCMs) as input forcing for future climate projections for future studies in this region.

The RUC simulation differs from REF in that it uses the RUC LSM (Smirnova et al, 2000), rather than the NOAH LSM (Chen and Dudhia, 2001a,b). This experiment was carried out as the choice of LSM can have a large influence on temperature and precipitation (e.g., Prabha et al, 2011; Mooney et al, 2012; Stéfanon et al, 2013). Whilst the NOAH LSM is the most commonly used LSM in WRF for regional climate modelling (e.g., Evans and McCabe, 2010; Argüeso et al, 2011; Awan et al, 2011; Argüeso et al, 2012), the RUC LSM is of comparable complexity but has not been as extensively evaluated.

The BMJ simulation differs from REF in that the BMJ scheme is used for convection rather than KF. The choice of convective scheme can have a strong influence on precipitation simulations (Bukovsky and Karoly, 2009; Argüeso et al, 2011; Awan et al, 2011). Whilst the majority of studies use the KF scheme (Bukovsky and Karoly, 2009; Evans and McCabe, 2010; Awan et al, 2011), Argüeso et al (2011) found the BMJ scheme performed better for their simulations. Experiments RRTMG and CAM consider different radiation schemes; RTG uses a modified version of the shortwave RRTM scheme for application in GCMs, RRTMG , for both longwave and shortwave radiation and the Community Atmosphere Model schemes are used for longwave and shortwave radiation in the CAM experiment. The accurate resolution of shortwave and longwave radiation is essential for modelling low level temperatures, and the PBL and the radiation schemes tested in this experiment tackle the problem in different ways. The CAM schemes use a Delta-Eddington approximation for shortwave radiation absorption and scattering (Collins et al, 2004), and the RRTMG model, like the RRTM model, uses the correlated-k method for radiative transfer (Iacono et al, 2008). Both CAM and RRTMG schemes use overlapping cloud fraction algorithms to determine the cloudiness of the grid whereas the RRTM/Dudhia parameterisaion considers only a binary measure of grid cloudiness. CAM and RRTMG radiation schemes differ further from Dudhia/RRTM in that they take into account the concentrations of trace gases, aerosols, ozone, and carbon-dioxide, and they consider reflected shortwave radiation fluxes.

PBL and land surface schemes are varied in experiments AC2 and AC2_P. These experiments differ from REF through the use of the AC2 scheme for PBL with the MO land surface scheme in the case of experiment AC2 and with the Pleim-Xiu (PX) surface layer scheme (Pleim, 2006) in experiment AC2_P. These experiments were undertaken as a result of Argüeso et al (2011) findings that the AC2 scheme performed better for their simulations as compared to the more widely used YSU/MO schemes. The PX scheme was also tested as the AC2 scheme can be used in conjunction with both the MO and PX schemes.

Simulations 3C and 5C_D test the sensitivity of microphysics schemes. The 3C experiment is the same as in REF, except it employs the simpler 3-class microphysics, rather than the more complex 5-class scheme used in REF. The 3-class scheme only resolves 3 states of cloud water, namely water/ice, vapour, and rain/snow, whereas the 5-class scheme includes cloud water and ice, rain, snow, and vapour. The 5C_D experiment employs the double moment 5-class scheme rather than the single moment scheme of the REF experiment. The double moment scheme computes hydrometeor number concentrations, allowing for more flexibility, whereas the single moment schemes have a pre-defined distribution function for hydrometeor sizes (Lim and Hong, 2009). As a rule of thumb, high resolution simulations of individual storm events usually require more complex microphysics parameterisations, which may not be necessary for regional climate runs (from a computational perspective) hence it is useful to test several schemes to strike the right balance. We note that more complex 6-class schemes exist in WRF which include graupel, however, this form of precipitation is rarely observed in SWWA, and hence these schemes were not tested.

The final two experiments, FNL_RTG and ERA_RTG, were conducted as a consequence of the results from the experiment RTG which will be discussed later. These simulations differ from the REF experiment because they employ the RRTMG radiation scheme (for both longwave and shortwave radiation), and they use the NCEP-FNL (FNL_RTG) and ERA-Int (ERA_RTG) lateral boundary conditions.

2.2 Observations, regionalisation and data analysis

Daily gridded observations of precipitation and maximum and minimum temperatures were obtained from the Australian Bureau of Meteorology (BoM) (Jones et al, 2009) as part of the Australian Soil Water Availability Project (AWAP) (Raupach et al, 2008, 2009). These data are at a resolution of $0.05^{o} \times 0.05^{o}$ (approximately 5 km $\times$ 5 km) and are obtained by interpolating data from a network of stations (Jones et al, 2009). The number of stations used varies with time and their location are shown as the white dots in Figs. 4a and 4b for precipitation and temperature respectively. The AWAP data-set has been previously used in evaluating climate simulations over Australia (Evans and McCabe, 2010; Evans et al, 2011). King et al (2013) evaluated the AWAP data-set against station observations for extreme rainfall events and found that whilst the product tends to underestimate the frequency of heavy rainfall events and overestimate that of very low rainfall events, it generally performs reasonably well in capturing the inter-annual variability of extreme rainfall events, and their spatial extents. The latter caution against the use of AWAP when the aim is to examine trends and variability in extremes in regions with poor coverage of station locations. This is not an issue for this study as the focus is on the ability of WRF to simulate the seasonal variation over a one year period.

An initial comparison of the WRF output to the BoM AWAP gridded data showed that the model had errors specific to particular land use regions within the model domain. Considering these particularities, we distinguish 3 regions as illustrated in Fig. 3; the coastal region, agricultural region and the predominantly inland rangelands. The northern reaches of the coastal region accommodates the overwhelming majority of the SWWA population in the Perth metropolitan area and the south and east of the region contains most of the remaining forest in the SWWA. The agricultural region, which consists almost exclusively of cereal crops in the winter and spring and bare earth for the remainder of the year, is physically bounded to the east by nature reserves and a vermin proof fence (Lyons et al, 1993), but it is constrained also by the rainfall gradient, which declines markedly from west to east as the distance from the coast increases (Fig. 4(a)). The eastern boundary of the agricultural region is therefore the approximate limit at which rain fed crops are viable. The rangelands region, which comprises the majority of the SWWA is a semi-arid to arid zone which is sparsely vegetated and remains in a relatively pristine state. As defined, these land use regions are particularly relevant for management of the agriculture and forestry sectors in the SWWA however they also represent different climatic regions, particularly with respect to rainfall; with the coastal region receiving the majority of the rainfall while the agricultural region receives on average about half the rainfall of the coast which is a combination of frontal and convective processes. Statistics were computed for each region (Fig. 3) after removing the relaxation zone from the grid boundaries, and shown in Taylor diagrams (Taylor, 2001) and bias plots (biases are shown in absolute and percentage terms, i.e., scaled by the mean of the observations).

Whilst the use of a gridded data-set such as AWAP is very useful in evaluating WRF, it has limited use in investigating the intensity, location, and frequency of rainfall events. To this end, we also selected 3 precipitation stations, one in each region, to carry out a time-series analysis. These stations are shown in Fig. 3 and were chosen because they are Bureau of Meteorology stations with long term quality controlled data and are on approximately the same latitude.

2.3 Climatology

The BoM-AWAP data is illustrated in Fig. 4 showing the seasonal mean summer (December-January-February or DJF), autumn (March-April-May or MAM), winter (June-July-August or JJA), and spring (September-October-November or SON) precipitation, maximum temperatures, and minimum temperatures for 2010. During DJF, precipitation is mostly confined inland and brought about by North-West cloud bands and surface convection. Precipitation increases during MAM and JJA as the cold-fronts associated with the sub-tropical high pressure cells move further North, with maximum precipitation during JJA and a distinct East-West gradient. Precipitation decreases on the West coast during SON as the cold-fronts move further South, and North-West cloud bands and convection lead to precipitation further inland. Maximum and minimum temperatures both show a North-South gradient, with the highest temperatures confined to the North-West and coolest temperatures to the South-West.

Figure 5 shows the seasonal anomalies for precipitation and maximum and minimum temperatures for 2010 over the period 1970-2010. 2010 was clearly a dryer than average year, especially during JJA (winter) and SON (spring), and warmer than average, especially in SON, DJF (summer), and MAM (autumn) during the day (maximum temperatures), but cooler than average in JJA during the night (minimum temperatures). This overall warming and drying trend has been observed since the mid 1970's from streamflow and station observations and been consistent to date (Bates et al, 2008). The overall warming and drying trend is also consistent with future climate projections for this region. Namely, Moise and Hudson (2008) conducted an analysis of IPCC AR4 coupled ocean-atmosphere GCMs, and found that all of them consistently predict a 25-30% decrease in winter rainfall for southwest Australia. The more recent IPCC AR5 report (Collins et al, 2013) also identifies SWWA as a region of strong agreement for decreases in maximum 5-day precipitation and increase in consecutive dry days. Hence, whilst the choice of 2010 does not constitute an average year in a climatological sense, it is representative of future changes in climate for this region. Since the aim of this study is to investigate a WRF configuration which will be used for regional climate projections, the choice of 2010 (dryer and warmer than average) is particularly relevant.

3 Results

Before analysing the influence of the different forcing data and physics options, we first briefly examine the effect of the use of the higher resolution 10-km inner nested grid as compared to the outer 50-km grid, as illustrated in Fig. 6 showing seasonal precipitation, maximum and minimum temperatures from the REF experiment for the two domains. The main influence of the inner nest is to better resolve coastal processes, especially for precipitation, with the outer domain clearly unable to capture much of the coastal rainfall as compared to the observations (Fig. 4). This is not unexpected as the topography is better resolved for the inner nest (Fig. 1). The influence of the inner 10-km grid on temperature is less evident as compared to precipitation, but similarly, the differences are mostly at the coast (for example JJA minimum temperatures). Both domains show very similar patterns and biases as compared to the observation (Fig. 4).

3.1 Temperature

Figures 7 and 8 show Taylor diagrams for maximum and minimum temperatures respectively (the coastal region is represented by squares, the agricultural region by triangles, and the rangelands by circles). The arc on the Taylor diagrams show the spatial correlation pattern, while the horizontal and vertical axes represent the ratio of the variance of the model to the observations. The dashed concentric circles represent the centred pattern root-mean-square (RMS) difference. Hence, for a perfect model, the point should lie on the 1:1 curved line (equal variance to the observations), and as close as possible to the horizontal axis (zero RMS difference and pattern correlation of one). Absolute and percentage biases are shown in Tables 2 and 3.

All simulations show high pattern correlation of 0.8 to 1.0 for maximum temperatures. The RMS errors and relative variances are higher during JJA (austral winter) as compared to the other seasons. Maximum temperatures are simulated well by the REF experiment in terms of correlation, RMS error, and variance however there is a systematic negative bias which is highest in DJF and SON, between 3-4 °C. There is considerable variation in the bias between the regions however, there is no consistency between the seasons in this regard; for example, the coastal region is simulated with the least bias in MAM but in SON the coastal bias exceeds that of both the agricultural region and rangelands. This may be partly due to the fact that the regionalisation used reflects the east-west precipitation gradient, whereas the temperature gradient is, as expected, north-south. This is clearly a shortfall of this study, and a separate regionalisation for temperature could be more appropriate. However, the context here is to provide future climate information to the agricultural and forestry sectors, and hence, we use a regionalisation based on broad land-use classes.

Reflecting the trend observed in maximum temperatures, night time minimum temperatures are also systematically underestimated by the REF experiment however there is considerably less variation in the bias between the coastal, rangeland and agricultural regions. The percentage bias is also greater for minimum temperatures than for maximum; biases were generally below 12% of maximum temperatures however minimum temperature biases are generally greater than 12%, and in some cases (the winter minima in the agricultural region and rangelands) bias exceeds 50%. The correlation of both minimum and maximum temperatures in the REF experiment were high, except for some simulations during JJA for the rangelands (low density of station observations) and the variance ratio was less than 2, showing good performance.

The N_SST experiment results were very similar to that of the REF experiment showing that use of NOAA SSTs rather than skin temperatures within NNRP has little influence on temperatures. The FNL and ERA simulations however, demonstrate significantly lower bias relative to the REF experiment, and all experiments driven by NNRP boundary conditions, for maximum temperatures, especially in the warmer months (DFJ, MAM and SON). Both simulations had a slight positive bias for minimum temperatures. While the correlations of these experiments are high, they do exhibit some noticeable differences in variance between models and observations when compared to the NNRP driven experiments, particularly with respect to minimum temperatures. For example, when compared to REF, RMS errors and the variance ratio are higher during DJF at the coast and in the agricultural regions. However, for impact studies focussing on agriculture and forestry, it is temperature extremes, rather than variability, which has the strongest impact. Hence, the reduction in bias is a major advantage of using the FNL and ERA-interim data-sets over the NNRP. We also note that while both sets of driving data perform better than NNRP, there is however little difference between the performance of these two re-analysis packages. Of particular relevance to agriculture is surface soil moisture and temperature and an examination of the differences between the 3 re-analysis showed that FNL and ERA had higher surface soil temperatures as compared to REF by 2-3 °C (not shown), reflecting the lower screen temperature bias for these two experiments as compared to REF (Tables 2 and 3). The FNL and ERA experiments also showed slightly higher soil moisture as compared to REF by about 0.05-0.1 m^{-3} m^{-3} which can be explained by the higher precipitation for these two experiments, discussed later in section 3.2.

The RUC experiment has large positive biases as compared to the REF experiment for maximum temperature ranging from 5 to 9°C especially during the SON, DJF, and MAM seasons (Table 2), whilst the biases for minimum temperature were slightly lower as compared to REF (Table 3). The Taylor diagram for maximum temperature (Fig. 7) shows that the RUC experiment had large variance ratios as well as RMS error, especially for JJA and SON, as compared to REF experiment, whilst there were no marked differences for minimum temperature (Fig. 8). Figure 9 shows the seasonal differences in sensible and latent heat flux between the REF and RUC experiments. During DJF and SON, the RUC experiment had higher sensible heat over most of the agricultural region and rangelands by about 15-30 W m^{-2} and lower latent heat flux by about 5-15 W m^{-2}, reflecting the large biases in maximum temperature. Differences in soil moisture between the two experiments were less than 0.1 m^{-3} m^{-3}.

The BMJ experiment results were very similar to the REF experiment, showing little change in bias or RMS and variance ratio or spatial correlation pattern. Changing the radiation scheme showed more interesting results. CAM shows a slight reduction in negative bias relative to the REF experiment however the improvement observed by the use of the RRTMG radiative scheme for longwave and shortwave radiation (in experiment RTG) is significant, and produces the strongest model performance across all simulations driven by NNRP boundary conditions. In MAM and JJA, the negative bias is almost eliminated entirely by the RTG experiment and there is at least a 1°C improvement in DJF and SON. It was as a result of these findings that the FNL_RTG and ERA_RTG model simulations were run to further assess the merits of the RRTMG scheme when used with the FNL and ERA-interim re-analyses.

When the FNL and ERA-Interim boundary conditions are used along with the RRTMG longwave and shortwave radiation schemes in experiments FNL_RTG and ERA_RTG, the results show a reduction in the negative bias for maximum temperatures, indicating some improvement as compared to to the FNL and ERA simulations (Table 2). For minimum temperatures, the FNL and ERA simulation had small positive biases, and use the RRTMG scheme results in an increase in these biases (Table 3), i.e., the net effect of the RRTMG scheme is warmer temperatures. For the REF experiment, the biases were mostly negative both maximum and minimum temperatures, and hence, the RTG simulation showed a reduction in bias for both maximum and minimum temperatures. For the FNL and ERA experiments, biases were negative for maximum temperature, but positive for minimum temperatures, and hence use of the RRTMG scheme in FNL_RTG and ERA_RTG improved the maximum temperature bias, but increased the minimum temperature bias. The net warming effect of the RRTMG scheme (in experiments RTG, FNL_RTG and ERA_RTG) can be explained by the high incoming shortwave radiation as compared to use of the Dudhia scheme (in experiments REF, FNL, and ERA) as illustrated in Fig. 10 showing differences between 15-30 W m^{-2} across the domain for all seasons.

Whilst the use of different micro-physics had little to no influence on temperature, the use of the AC2 PBL scheme increased the negative bias for maximum temperatures, most notably in DJF, MAM, and SON, especially in the rangelands region. This negative bias is further enhanced when the AC2 PBL scheme is employed in combination with the Pliem Xu surface layer scheme (experiment AC2_P). However, for maximum temperatures, the AC2_P simulations result in lower biases as compared to the AC2 experiment, during DJF and SON. The high negative bias for minimum temperatures can be related to a rapid collapse of the nocturnal PBL as illustrated in Fig. 11, showing the seasonal daily average minimum PBL height for the AC2, AC2_P and REF experiments.

3.2 Precipitation

Figure 12 shows Taylor diagrams for precipitation and the absolute and percentage biases are shown in Table 4. A clear seasonal pattern is evident for all simulations and regions, with biases, RMS errors and ratio of variances being generally higher during DJF and MAM (austral summer and autumn) and lower during JJA and SON (winter and spring). The weak performance in precipitation for all simulations during summer can be attributed to the difficulty in accurately simulating the intensity of the convective rainfall events which dominate rainfall in summer and autumn, especially in the rangelands region. Winter rain is mostly from frontal systems, i.e., synoptically driven and strongly influenced by the forcing data, and hence, JJA and SON precipitation show lower errors.

Biases for the REF experiment are negative except for coastal region during DJF (low rainfall season), showing the WRF generally under-predicts precipitation, and additionally, the bias is most negative for the rangelands regions, ranging from -80 to -100 % (a bias of -100% indicates that the model hardly captured any of the observed rainfall). Precipitation in this region is relatively small in magnitude compared to the coast (see Figure 4) and strongly influenced by surface convection all year-round, rather than synoptically driven. Given the spatial paucity of the observational network in the rangelands there is an inherent disconnect between the observation of small scale convective storms and the model's ability to simulate such events.

The spatial correlations varied generally between 0.8 and 1.0, showing that WRF reproduced spatial patterns of precipitation reasonably well. Frontal rainfall, which is the source of most of the precipitation along the coast and in the agricultural region in JJA (Fig. 12c) and SON (Fig. 12d), is well simulated however the negative bias in the REF simulation is not insignificant, particularly in the agricultural areas (55%). Previous studies in the SWWA have highlighted the meteorological importance of the Darling scarp (a sloping, 300m high escarpment, 25km inland which runs parallel to the north-south coastline) and the need to run simulations at a very fine scale to capture the influence on precipitation of this topographical feature (Pitts and Lyons, 1990; Kala et al, 2010). Hence, it is likely that the resolution of this simulation is not accounting for the influence of the scarp on frontal rainfall.

To better quantify the ability of WRF to simulate the intensity, timing, and frequency of rainfall events, we carried out a station-level comparison of the REF simulated precipitation against 3 stations (Fig. 3), one located in each region and at roughly the same latitude, illustrated in Fig. 13. Close to the coast, the timing of rainfall events is very well captured, with the exception of a large rainfall event in late March, and WRF generally under-predicts precipitation. Within the agricultural and rangelands region, as the intensity of rainfall decreases further from the coast, the REF experiment clearly is unable to capture small rainfall events, especially at the Norseman station. Namely, REF only simulated 3 rainfall events, whereas the observations show well in excess of 15 rainfall events.

The use of the NOAA SSTs in the N_SST experiment as compared to the REF experiment results in a reduction in bias for precipitation along the coast and to a lesser degree in the agricultural region during JJA and SON. There is a large increase in percentage bias at the coast and the agricultural region during DJF, however, this corresponds to a very small change in absolute bias. This is expected as DJF rainfall in these regions is relatively small. Figure 2 shows the difference in SST between the N_SST and REF experiments during JJA and SON, and illustrates that the use of surface skin temperature data in the REF experiment as a surrogate for SST is predominantly underestimating SST, especially close to the coast. In terms of winter precipitation, there is merit in employing the satellite derived NOAA SST data as used in the N_SST experiment, especially when simulation domains contain a significant percentage of sea surface, as is the case here. While the NOAA SSTs are providing a benefit in winter coastal model performance, it is however worth noting that, in addition to a slight bias increase in DJF, the N_SST simulation did result in an increase in relative variance and RMS errors for precipitation in the warmer months of DJF and MAM. For this region, accurate simulations of precipitation along the coast during JJA is of prime importance as it is the main source of water for rain-fed agriculture. Hence, we argue that the use of NOAA SSTs is a better option.

The FNL and ERA simulations show a clear improvement in bias during MAM, JJA, and SON, as compared to the REF experiment. This is especially noticeable for the rangelands region, with smaller biases during JJA and SON as compared to much larger and negative (close to -100%) bias for the REF experiment. During DJF, the FNL simulation produces a larger bias for the coastal and agricultural regions, as compared to the REF experiment, while the ERA simulation only improves the bias at the coast. However both the ERA and FNL simulations shows higher spatial correlation pattern and lower variance ratio and RMS errors as compared to the REF experiment, but the ERA simulations performs best overall. An examination of the differences in SST between the REF and ERA and REF and FNL simulations did not reveal any clear spatial patterns which could explain the differences in precipitation simulations.

Use of the RUC LSM had little influence on precipitation as compared to REF, except for higher RMS error and variance ratio at the coast for MAM and larger negative bias at the coast during JJA. It was interesting to note that although RUC produced less precipitation than REF, as shown by the larger negative bias, the RUC simulations had larger latent heat flux during JJA at the coast, a counter-intuitive result. This suggests that the RUC LSM has a larger evaporative flux as compared to the NOAH LSM when soil water is available (i.e., during MAM and JJA), which could be due to the different treatment of above ground processes (e.g., vegetation evaporation), surface processes (e.g., run-off), as well was sub-surface processes (root zone drainage) between the two LSMs. To adequately quantify these differences would required running both LSMs offline with the same forcing, which is outside of the scope of this paper.

The BMJ simulation had fairly similar biases compared to the REF (which uses the KF scheme) experiment during DJF but smaller ratio of variance and RMS errors, showing a better simulation of variability of precipitation. During MAM, JJA, and SON, the BMJ simulation had higher (more negative) bias at the coast as compared to the REF experiment, but lower variance ratio. Hence, both the KF and BMJ schemes have their merits and disadvantages. However the higher bias during JJA and SON at the coast is not insignificant (almost double) and as such, it appears that the KF scheme may be more appropriate in this case. The RTG and CAM simulations had similar biases to REF, except that the bias at the coast during SON was almost twice as large. SON is the austral spring, and represents a transition from frontal (synoptically driven) precipitation, to the summer regime when surface convection has a larger role. Hence, it appears that the radiation schemes are particularly sensitive during that transition period.

The AC2 and AC2_P simulations produced similar results during DJF and MAM, but both simulations had lower bias during JJA at the coast as compared to REF, and the AC2_P simulation showed a slight improvement in bias during SON at the coast. There were no major differences in the variance ratios, RMS errors, and spatial correlations. Similarly, the 3C and 5C_D simulations produced very similar results to the REF experiment for precipitation, i.e., the use of a simpler and less computationally expensive microphysics scheme (3C) appears to be appropriate.

The FNL_RTG and ERA_RTG schemes were conducted as result of an improvement in bias in maximum and minimum temperature when comparing the RTG to the REF simulation discussed earlier in section 3.1. The FNL_RTG and ERA_RTG produced very similar results for precipitation during JJA and SON as compared to the FNL and ERA simulations respectively, but there was a marked increase in bias at the rangelands during DJF and MAM. Namely, the precipitation bias increased from 9.5 and 5.8 mm month^{-1} during DJF and MAM at the rangelands for the FNL experiment, to 22.3 and 19.0 mm month^{-1} for the FNL_RTG experiment, and from 8.9 and 9.6 mm month^{-1} to 21.3 and 25.3 mm month^{-1} for the ERA as compared to the ERA_RTG experiment (Table 4). However, no such increase in bias was observed for the RTG experiment as compared to the REF experiment, showing that the RRTMG scheme results in different behaviour with different sources of driving data. We further explored this by examining the changes in convective available potential energy (CAPE), lifting condensation level (LCL), and precipitable water (PW) between the REF, FNL, and ERA simulations (i.e., using the Dudhia/RRTM shortwave/longwave schemes) and the RTG, FNL_RTG, and ERA_RTG (i.e., using the RRTMG/RRTMG shortwave/longwave scheme), as illustrated in Fig. 14. Use of the RRTMG scheme clearly results in an increase in CAPE between 60-140 J kg^{-1} during DJF and MAM for the FNL_RTG and ERA_RTG simulations as compared to FNL and ERA respectively, whilst the differences in CAPE between RTG as compared to REF is much smaller. Higher CAPE implies larger positive buoyancy and higher likelihood of convection and associated precipitation. Additionally, use of the RRTMG scheme clearly resulted in lower LCL and higher PW for all seasons within the rangelands for the FNL_RTG and ERA_RTG simulations as compared to FNL and ERA respectively. Hence, the increased positive buoyancy, lower LCL and larger amount of PW can explain the large positive precipitation biases.

4 Discussion

The REF experiment provided a reasonable simulation at the seasonal scale for the domain of the interest. However, the negative biases for maximum and minimum temperatures are not insignificant, given that impacts on agriculture and forestry are not only dependant on precipitation, but also temperature extremes (van Gool and Vernon, 2005; Lobell et al, 2012). Additionally, given the known issues of low moisture availability within the NNPR data-set for the southern hemisphere (Schneider et al, 2013), this combined with negative temperature biases, may partly explain the overall negative bias in precipitation as well. The temperature biases were reduced when using the FNL and ERA-interim re-analyses as forcing data. The better performance when using the ERA-interim and FNL re-analysis as compared to the NNRP is not unexpected, as the former have higher resolution, use more observational data and involve more accurate representations of the hydrological cycle (Dee et al, 2011). The better performance of ERA-Interim over NNRP has also been shown by Fersch et al (2012), who compared terrestrial water storage from WRF simulations over Australia (amongst other regions) with both re-analysis against remotely sensed estimates and showed that ERA-Interim driven simulations had lower biases as compared to NNRP, which had a dry tendency. This is in-line with our results which showed large negative biases in precipitation during winter for REF, but smaller positive biases for the ERA simulation. However, it must be noted that the resolution of NNRP is closer to that of GCMs and using NNRP may be more appropriate to enable comparisons with GCM forced simulations. However, if the focus is to re-produce the past climate as accurately as possible, then the use of ERA-Interim and FNL is more appropriate. The N_SST simulation, which used satellite derived SSTs with the NNRP re-analysis improved the bias for winter precipitation, showing that care should be taken in using the best available source of SST. This is in line with other studies which have shown that the accurate prescription of SSTs in WRF is critical to simulating extreme precipitation events over eastern Australia (Evans and Boyer-Souchet, 2012). An important source of uncertainly for future climate projections are biases within GCMs used to drive RCMs. Whilst this study did not use any GCM data, the results presented also suggest that any future climate study has to use data from more than one GCM, and additionally, critically examine inherent uncertainties and biases within the driving data used.

Use of the RUC land surface model resulted in large positive biases for maximum temperature, especially during the warmer seasons of SON (spring) and DJF (summer). Similar results have been found by Mooney et al (2012) over Europe, with the RUC LSM having a bias for the mean summer air temperature of up to 5 °C whilst the NOAH LSM showed much lower biases (with all other physics options being the same). The biases reported here are higher, ranging from 6 to 10 °C (Table 2), since we explicitly focussed on maximum and minimum temperatures, while Mooney et al (2012) evaluated the mean temperature. Mooney et al (2012) also reported that the NOAH LSM has a greater tendency to show a positive bias in daily precipitation as compared to the RUC. Here we also find that the NOAH LSM generally results in higher precipitation as compared to RUC with the NOAH LSM having a smaller negative bias as compared to RUC (Table 4). Comparison of the surface turbulent heat fluxes showed that the RUC LSM has higher sensible heat flux as compared to the NOAH LSM for DJF and SON, which can explain the temperature bias. However surface heat fluxes are integrative of processes with the PBL, and identifying the reasons behind the differences in surface fluxes between the RUC and NOAH LSMs would require running both models offline with the same forcing, which is beyond the scope of this paper.

Because of the predominance of convective rainfall, especially during summer months and the results of previous studies (Flaounas et al, 2011; Crétat et al, 2011), it was expected that simulated rainfall would be sensitive to different convective and PBL parameterisation schemes. However, we did not find large differences in simulated precipitation when switching from the KF to the BMJ cumulus schemes and from the YSU/MO to the AC2 and AC2_P PBL/Surface layer schemes. This may be due to several reasons. Firstly, we simulated a single year, which was particularly dry. However, whilst our results may be sensitive to the choice of year, the persistent warming and drying trend for this region, from both observations (Bates et al, 2008) and GCM projections (Moise and Hudson, 2008; Collins et al, 2013), gives us confidence that the choice of cumulus and PBL schemes have little influence on precipitation for SWWA. Secondly, the amount of convective rainfall during DJF in SWWA, is relatively small, compared to JJA (winter) precipitation, and this may also explain the lack of sensitivity to the different schemes, as previous studies have shown that the influence of different physics options is largest for more extreme precipitation events (Evans et al, 2011), and when focussing explicitly on mesoscale convective events (e.g., Jankov et al, 2005). Conversely, the lack of rainfall sensitivity to microphysics scheme was in line with previous research (Argüeso et al, 2011) and it appears that the simple 3-class single moment micro-physics scheme is sufficient, at least for this region and for such resolution. The most important shortfall remains the accurate simulation of DJF (summer) precipitation, which is not unexpected based on studies for similar meteorological conditions in other regions (Pohl et al, 2011)

Of particular note for the precipitation results is the fact that all the simulations demonstrate a consistent pattern in the predictive performance of WRF based on the regional groupings; the coastal region is simulated with the greatest skill and the rangelands with the least skill. The potential mechanisms for this pattern include a model response to the rainfall gradient, differences in the type of rainfall, change in land use type or a reduction in the distribution of rainfall monitoring stations. Based on the consistently high density of observations in both the coastal and agricultural regions (Fig 4a), it seems unlikely that observation error is solely responsible for this trend. However, because of the low density of observations in the rangelands, it is probable that the error in this region has been exacerbated by some observational errors, which we are unable to quantify.

The sensitivity of WRF to different radiation schemes yielded interesting results. Namely, whilst the model was not very sensitive to the use of the CAM radiation scheme, it was shown to be sensitive to the RRTMG scheme. RRTMG increased the minimum and maximum temperatures relative to simulations using the RRTM/Dudhia scheme due to higher incoming shortwave radiation for all seasons. This improved the bias with NNRP driven simulation, as the latter had negative biases for both maximum and minimum temperatures. However, use of the RRTMG scheme degraded performance for minimum temperatures when used with NCEP-FNL or ERA-interim, as the increase in incoming shortwave radiation acted to make the small positive biases even larger. The higher incoming shortwave radiation could be explained by the fact that the RRTMG scheme allows for fractions to be applied to sub grid cloud cover, unlike the Dudhia scheme where a grid is either completely cloudy or clear. Similar results have been reported elsewhere. Namely, Evans et al (2011) conducted a WRF physics ensemble over eastern Australia (they use ERA-Interim) and also found that the RRTMG/RRTMG shortwave/longwave scheme generally overestimated temperatures. The RRTMG scheme also resulted in large bias in precipitation in the rangelands during the warmer seasons of DJF and MAM when used with NCEP-FNL and ERA-interim forcing, whereas this was not observed when using NNRP. This was due to the RRTMG scheme resulting in much larger CAPE when used with NCEP-FNL and ERA-Interim data as compared to NNRP. This in conjunction with lower LCL and higher precipitable water, would have led to increased precipitation. Evans et al (2011) also found that the RRTMG radiation, KF cumulus, and YSU PBL physics combination performed consistently poorly for all their simulations of storm events in Eastern Australia. Moreover, sensitivity studies over other regions (Yuan et al, 2012; Pohl et al, 2011; Awan et al, 2011), have found that shortwave radiation schemes in particular, have a strong precipitation response. Hence our results are consistent with previous studies.

Changing PBL schemes had a strong influence on temperatures. Namely, use of the AC2 PBL scheme, especially in conjunction with the PX surface layer scheme is clearly not recommended for our domain, due to large biases in minimum temperatures in the rangelands region. While both YSU and AC2 utilise non local closure schemes, AC2 reverts to a local closure scheme under conditions of neutrality or stability, especially at night (Hu et al, 2010). As a consequence of this switch to a local closure scheme, the AC2 PBL scheme has a tendency to suffer from a lack of mixing in the night-time boundary layer, which results in a too rapid collapse, low minimum PBL and hence negative bias with respect to night-time minimum temperatures. Hence, this mechanism can explain the high biases.

Whilst the choice of PBL schemes has been shown to influence precipitation simulations in other studies (e.g., Argüeso et al, 2011), this was not the case here. Studies in the SWWA have demonstrated that land cover change can impact boundary layer development and therefore precipitation in the region (Lyons, 2002; Kala et al, 2010; Nair et al, 2011). While each region does demonstrate markedly different land uses, and in the case of the agricultural region extensive land cover change, for these land uses to be influencing precipitation, it was expected that this would be demonstrated through a sensitivity to PBL and surface layer scheme, which was not observed. That the choice of PBL scheme does not appear to influence rainfall sensitivity suggests that the errors in rainfall simulation and the regional differences in model performance are not strongly associated with land use type.

5 Conclusions

We carried out a range of sensitivity experiments with WRF, using different forcing data and model physics options. The aim of this was to better inform the planning of future long-term regional climate simulations for this region with significant agricultural and forestry sectors. Overall, it is clear the control (REF) simulation experimental set-up is adequate for longer term climatic simulations for this region, at least at the seasonal time-scale and 10-km spatial resolution. An important issue remains the systematic underestimation of precipitation at the coast, which could be due to un-resolved topography, and hence future studies should aim at further quantifying the role of the Darling scarp on orographically induced precipitation in SWWA. The lack of precipitation during summer further from the coast suggests land-atmosphere feedbacks are not being adequately captured, and this also requires further investigation. The simulations with different re-analysis products show that when the goal is to establish a base-line climatology, the ERA-interim data-set should be preferred over the FNL and NNRP. When NNRP is nonetheless used, the use of NOAA SSTs should be preferred over the use of surface skin temperatures within the NNRP data-set.

Our results show that the choice of PBL scheme can have a large influence on temperatures, and choice of radiation scheme on both temperatures and precipitation in SWWA. Consistent with previous studies, we found that the RRTMG, in combination with the YSU PBL scheme, and KF cumulus scheme is not recommended. Additionally, the AC2 PBL scheme results in large biases for minimum temperature, and should not be used, at least for the domain of interest here. The KF and BMJ cumulus scheme did not result in significant differences for our domain, and consistent with several studies, using more complex micro-physics does not improve precipitation simulations. More interestingly, we show that schemes may behave differently with different forcing data-sets, as was shown with the RRTMG radiation scheme. Hence, sensitivity testing should ideally include both use of different physics options as well as forcing data.

Future studies will evaluate WRF driven by the ERA-interim re-analysis on a climatic (30 years) time-scale (similar to the ERA simulation here), and evaluate the model at daily, seasonal, and inter-annual time-scales, and additionally, use station and sounding observations, in addition to the AWAP gridded product. This will in turn be used to help inform the design of GCM forced simulations to provide regional information of possible future climatic changes in SWWA.

Acknowledgements This research is funded by the Australian Grains Research and Development Grant (MCV00013). All WRF simulations were supported by iVEC (http://www.ivec.org/) through the use of advanced computing resources provided by the Pawsey Super-Computing Centre located at Murdoch University, Perth, Western Australia, through the National Computational Merit Allocation Scheme. Jatin Kala is supported by the Australian Research Council Centre of Excellence for Climate System Science (CE110001028). Julia Andrys is supported by an Australian Postgraduate Award and a Grains Industry Research Scholarship. NOAA_OI_SST_V2 data were provided by the NOAA/OAR/ESRL PSD, Boulder, Colorado, USA, from their Web site at http://www.esrl.noaa.gov/psd/. The NNRP and NCEP-FNL data for this study are from the Research Data Archive (RDA) which is maintained by the Computational and Information Systems Laboratory (CISL) at NCAR. NCAR is sponsored by the National Science Foundation (NSF). The original data are available from the RDA (http://dss.ucar.edu) in dataset number ds090.0 and ds083.2 respectively. ERA-interim data were obtained from the ECMWF data server (http://data-portal.ecmwf.int/data/d/interim_daily/). The comments of two anonymous reviews helped to further enhance the quality of this manuscript. All this support is gratefully acknowledged.

References

ABS (2010) Australian Bureau of Statistics (ABS) Year Book: Agriculture, Available online at: http:www.abs.gov.au

Andrich MA, Imberger J (2013) The effect of land clearing on rainfall and fresh water resources in western australia: a multi-functional sustainability analysis. International Journal of Sustainable Development and World Ecology 20:549–563, DOI 10.1080/13504509.2013.850752

Argüeso D, Hidalgo-Muñoz J, Gámiz-Fortis SR, Esteban-Parra MJ, Dudhia J, Castro-Díez Y (2011) Evaluation of WRF parameterizations for climate studies over southern spain using a multistep regionalization. Journal of Climate 24:5633–5651, DOI 10.1175/JCLI-D-11-00073.1

Argüeso D, Hidalgo-Muñoz JM, Gámiz-Fortis SR, Esteban-Parra MJ, Castro-Díez Y (2012) High-resolution projections of mean and extreme precipitation over spain using the wrf model (2070–2099 versus 1970–1999). Journal of Geophysical Research: Atmospheres 117(D12), DOI 10.1029/2011JD017399

Awan NK, Truhetz H, Gobiet A (2011) Parameterization-induced error characteristics of MM5 and WRF operated in climate mode over the Alpline region: An ensemble-based analysis. Journal of Climate 24:3107–3123

Bates B, Hope P, Ryan B, Smith I, Charles S (2008) Key findings from the indian ocean climate initiative and their impact on policy development in australia. Climatic Change 89:339–354, DOI 10.1007/s10584-007-9390-9

Betts AK (1986) A new convective adjustment scheme. Part I: Observational and theoretical basis. Quarterly Journal of the Royal Meteorological Society 112:677–691

Betts AK, Miller MJ (1986) A new convective adjustment scheme. Part II: Single column tests using GATE wave, BOMEX, ATEX and arctic air-mass data sets. Quarterly Journal of the Royal Meteorological Society 112:693–709

Bowden JH, Otte TL, Nolte CG, Otte MJ (2011) Examining interior grid nudging techniques using two-way nesting in the WRF model for regional climate modeling. Journal of Climate 25:2805–2823, DOI 10.1175/JCLI-D-11-00167.1

Bukovsky MS, Karoly DJ (2009) Precipitation simulations using WRF as a nested regional climate model. Journal of Applied Meteorology and Climatology 48:2152–2159, DOI 10.1175/2009JAMC2186.1

Bukovsky MS, Karoly DJ (2011) A regional modeling study of climate change impacts on warm-season precipitation in the central U.S. Journal of Climate 24:19852002, DOI 10.1175/2010JCLI3447.1

Caldwell P, Chin HN, Bader D, Bala G (2009) Evaluation of a WRF dynamical downscaling simulation over california. Climatic Change 95:499–521, 10.1007/s10584-009-9583-5

Chen F, Dudhia J (2001a) Coupling an advanced land surface–hydrology model with the Penn State–NCAR MM5 modeling system. Part I: Model implementation and sensitivity. Monthly Weather Review 129:569–585, DOI 10.1175/1520-0493(2001)129¡0569:CAALSH¿2.0.CO;2

Chen F, Dudhia J (2001b) Coupling an advanced land surface–hydrology model with the Penn State–NCAR MM5 modeling system. Part II: Preliminary model validation. Monthly Weather Review 129:587–604, DOI 10.1175/1520-0493(2001)129¡0587:CAALSH¿2.0.CO;2

Collins RK M, Arblaster J, Dufresne JL, Fichefet T, Friedlingstein P, Gao X, Gutowski W, Johns T, Krinner G, Shongwe M, Tebaldi C, Weaver A, Wehner M

(2013) Long-term Climate Change: Projections, Commitments and Irreversibility. In: Climate Change 2013: The Physical Science Basis. Contribution of Working Group I to the Fifth Assessment Report of the Intergovernmental Panel on Climate Change [Stocker, T.F., D. Qin, G.-K. Plattner, M. Tignor, S.K. Allen, J. Boschung, A. Nauels, Y. Xia, V. Bex and P.M. Midgley (eds.)]. Cambridge University Press, Cambridge, United Kingdom and New York, NY, USA. http://www.climatechange2013.org/images/report/WG1AR5_Chapter12_FINAL.pdf

Collins WD, Rash PJ, Boville BA, Hack JJ, McCaa JR, Williamson DL, Kiehl JT, Briegleb B (2004) Description of the NCAR Community Atmosphere Model (CAM 3.0). NCAR Technical Note NCAR/TN-464+STR, 266 pp., NCAR

Crétat J, Pohl B, Richard Y, Drobinski P (2011) Uncertainties in simulating regional climate of Southern Africa: sensitivity to physical parameterizations using WRF. Climate Dynamics 38:613–634, DOI 10.1007/s00382-011-1055-8

Dee DP, Uppala SM, Simmons AJ, Berrisford P, Poli P, Kobayashi S, Andrae U, Balmaseda MA, Balsamo G, Bauer P, Bechtold P, Beljaars ACM, van de Berg L, Bidlot J, Bormann N, Delsol C, Dragani R, Fuentes M, Geer AJ, Haimberger L, Healy SB, Hersbach H, Hólm EV, Isaksen L, Kållberg P, Köhler M, Matricardi M, McNally AP, Monge-Sanz BM, Morcrette JJ, Park BK, Peubey C, de Rosnay P, Tavolato C, Thépaut JN, Vitart F (2011) The ERA-interim reanalysis: configuration and performance of the data assimilation system. Quarterly Journal of the Royal Meteorological Society 137:553–597, DOI 10.1002/qj.828

Dudhia J (1989) Numerical study of convection observed during the winter monsoon experiment using a mesoscale two-dimensional model. Journal of Atmospheric Science 46:3077–3107

Ek MB, Mitchell KE, Lin Y, Rogers E, Grunmann P, Koren V, Gayno G, Tarpley JD (2003) Implementation of Noah land surface model advances in the National Centers for Environmental Prediction operational mesoscale Eta model. Journal of Geophysical Research 108(D22), DOI 10.1029/2002JD003296

Evans BJ, Lyons T (2013) Bioclimatic extremes drive forest mortality in southwest, Western Australia. Climate 1:28–52, DOI 10.3390/cli1020028

Evans JP, Boyer-Souchet I (2012) Local sea surface temperatures add to extreme precipitation in northeast Australia during La Niña. Geophysical Research Letters 39(10), DOI 10.1029/2012GL052014

Evans JP, McCabe MF (2010) Regional climate simulation over Australia's Murray-Darling basin: A multitemporal assessment. Journal of Geophysical Research 115:D14,114, DOI 10.1029/2010JD013816

Evans JP, Ekström M, Ji F (2011) Evaluating the performance of a WRF physics ensemble over South-East Australia. Climate Dynamics 39:1241–1258, DOI 10.1007/s00382-011-1244-5

Fersch B, Kunstmann H, Bárdossy A, Devaraju B, Sneeuw N (2012) Continental-scale basin water storage variation from global and dynamically downscaled atmospheric water budgets in comparison with GRACE-derived observations. Journal of Hydrometeorology 13:1589–1603, DOI 10.1175/JHM-D-11-0143.1

Flaounas E, Bastin S, Janicot S (2011) Regional climate modelling of the 2006 west African monsoon: sensitivity to convection and planetary boundary layer parameterisation using WRF. Climate Dynamics 36:1083–1105

Gentilli J (1971) Australian Climate Patterns. Thomas Nelson (Australia) Limited, 285 pp.

Giorgi F, Jones C, Asrar GR (2009) Addressing climate information needs at the regional level: the CORDEX framework. WMO Bulletins 58:175–183

van Gool D, Vernon L (2005) Potential impacts of climate change on agriculture and land use suitability: Wheat. Government of Western Australia, Department of Agriculture and Food, Resource Management Technial Report 295

Hong SY, Noh Y, Dudhia J (2006) A new vertical diffusion package with an explicit treatment of entrainment processes. Monthly Weather Review 134:2318–2341

Hu XM, Nielsen-Gammon JW, Zhang F (2010) Evaluation of Three Planetary Boundary Layer Schemes in the WRF Model. Journal of Applied Meteorology and Climatology 49:1831–1844, DOI 10.1175/2010JAMC2432.1

Huang X, Lyons TJ, Smith RCG (1995) Meteorological impact of replacing native perennial vegetation with annual agricultural species. Hydrological Processes 9:645–654

Hughes L (2003) Climate change and Australia: trends, projections and impacts. Austral Ecology 28:423–443

Hughes L, Westoby M, Cawsey EM (1993) Climate range sizes of *Eucalyptus* species in relation to future climate change. Global Ecology and Biogeography Letters 5:23–29

Hutchinson MF, Stein JA, Stein JL (2009) Geodata 9 second digital elevation model (dem-9s) version 3. http://www.ga.gov.au/

Iacono MJD, Mlawer JS, Shephard EJ, Clough MW, Collins SA, D W (2008) Radiative forcing by long-lived greenhouse gases: Calculations with the AER radiative transfer models. Journal of Geophysical Research 112:D13

Janjić ZI (1994) The step-mountain Eta coordinate model: Further developments of the convection, viscous sublayer, and turbulence closure schemes. Monthly

Weather Review 122:927–945

Janjić ZI (2000) Comments on “development and evaluation of a convection scheme for use in climate models”. Journal of Atmospheric Science 57:3686–3686

Jankov I, Gallus WA, Segal M, Shaw B, Koch SE (2005) The impact of different WRF model physical parameterizations and their interactions on warm season MCS rainfall. Weather and Forecasting 20:1048–1060, DOI 10.1175/WAF888.1

Jin J, Miller NL, Schlegel N (2010) Sensitivity study of four land surface schemes in the WRF model. Advances in Meteorology 2010:11 pages, DOI 10.1155/2010/167436

Jones DA, Wang W, Fawcett R (2009) High-qaulity spatial climate data-sets for Australia. Australian Meteorological and Oceanographic Society Journal 58:233–248

Kain JS (2004) The Kain–Fritsch convective parameterization: An update. Journal of Applied Meteorology and Climatology 43:170–181

Kala J, Lyons TJ, Nair US (2010) Numerical Simulations of the Impacts of Land-Cover Change on Cold Fronts in South-West Western Australia. Boundary-Layer Meteorology 138:121–138, DOI 10.1007/s10546-010-9547-3

Kalnay E, Kanamitsu M, Kistler R, Collins W, Deaven D, Gandin L, Iredell M, Saha S, White G, Woollen J, Zhu Y, Chelliah M, Ebisuzaki W, Higgins W, Janowiak J, Mo KC, Ropelewski C, Wang J, Leetmaa A, Reynolds R, Jenne R, Joseph D (1996) The NCEP/NCAR 40-year reanalysis project. Bulletin of the American and Meteorological Society 77:437–471

Kim EJ, Song SY (2010) Impact of air-sea interaction on East Asian summer monsoon climate in WRF. J Geophys Res 115:D19,118, DOI 10.1029/2009JD013253

King AD, Alexander LV, Donat MG (2013) The efficacy of using gridded data to examine extreme rainfall characteristics: a case study for australia. International Journal of Climatology 33:2376–2387, DOI 10.1002/joc.3588

Leung LR, Qian Y (2009) Atmospheric rivers induced heavy precipitation and flooding in the western U. S. simulated by the WRF regional climate model. Geophysical Research Letters 36:L03,820, DOI 10.1029/2008GLO036 445

Liang XZ, Choi HI, Kunkel KE, Dai Y, Joseph E, Wang JXL, Kumar P (2005) Surface boundary conditions for mesoscale regional climate models. Earth Interactions 9(18):1–28

Lim KSS, Hong SY (2009) Development of an effective double-moment cloud microphysics scheme with prognostic Cloud Condensation Nuclei (CCN) for weather and climate models. Monthly Weather Review 138:1587–1612

Liu P, Tsimpidi AP, Hu Y, Stone B, Russell AG, Nenes A (2012) Differences between downscaling with spectral and grid nudging using WRF. Atmospheric Chemistry and Physics 12:3601–3610, DOI 10.5194/acp-12-3601-2012

Lo JCF, Yang ZL, Pielke RA (2008) Assessment of three dynamical climate downscaling methods using the Weather Research and Forecasting (WRF) model. Journal of Geophysical Research 113:D09,112, DOI 10.1029/2007JD009216

Lobell DB, Sibley A, Ivan Ortiz-Monasterio J (2012) Extreme heat effects on wheat senescence in india. Nature Climate Change 2:186–189

Lyons TJ (2002) Clouds prefer native vegetation. Meteorology and Atmospheric Physics 80:131–140, DOI 10.1007/s007030200020

Lyons TJ, Huang X, Schwerdtfeger P, Hacker JM, Foster IJ, Smith RCG (1993) Land–Atmosphere Interaction in a Semiarid Region: The Bunny Fence Experiment. Bulletin of the American Meteorological Society 74:1327–1334, DOI

10.1175/1520-0477(1993)074¡1327:LIIASR¿2.0.CO;2

Ma Y, Lyons TJ (2000) Numerical simulation of a sea-breeze under dominant synoptic conditions at Perth. Meteorol Atmos Phys 73:89–103

Ma Y, Lyons TJ, Blockley JA (2001) Surface influences on the australian west coast trough. Meteorol Atmos Phys 68:207–217

Mlawer EJ, Taubman SJ, Brown PD, Iacono MJ, Clough SA (1997) Radiative transfer for inhomogeneous atmospheres: RRTM, a validated correlated-k model for the longwave. Journal of Geophysical Research 102(D14):16,663–16,682, DOI 10.1029/97JD00237

Moise AF, Hudson DA (2008) Probabilistic predictions of climate change for Australia and southern Africa using the reliability ensemble average of IPCC CMIP3 model simulations. Journal of Geophysical Research: Atmospheres 113(D15), DOI 10.1029/2007JD009250

Mooney PA, Mulligan FJ, Fealy R (2012) Evaluation of the sensitivity of the weather research and forecasting model to parameterization schemes for regional climates of Europe over the period 1990–95. Journal of Climate 26:1002–1017, DOI 10.1175/JCLI-D-11-00676.1

Nair US, Wu Y, Kala J, Lyons TJ, Pielke Sr RA, Hacker JM (2011) The role of land use change on the development and evolution of the west coast trough, convective clouds, and precipitation in southwest Australia. Journal of Geophysical Research 116(D7):D07,103, DOI 10.1029/2010JD014950

Omrani H, Drobinski P, Dubos T (2013) Optimal nudging strategies in regional climate modelling: investigation in a big-brother experiment over the European and Mediterranean regions. Climate Dynamics 41:2451–2470, DOI 10.1007/s00382-012-1615-6

Pitts RO, Lyons TJ (1989) Airflow over a two-dimensional escarpment. I: Observations. Quarterly Journal of the Royal Meteorological Society 115:965–981, DOI 10.1002/qj.49711548810

Pitts RO, Lyons TJ (1990) Airflow over a two-dimensional escarpment. II: Hydrostatic flow. Quarterly Journal of the Royal Meteorological Society 116(492):363–378, DOI 10.1002/qj.49711649207

Pleim JE (2006) A simple, efficient solution of flux–profile relationships in the atmospheric surface layer. Journal of Applied Meteorology and Climatology 45:341–347

Pleim JE (2007a) A combined local and nonlocal closure model for the atmospheric boundary layer. Part I: Model description and testing. Journal of Applied Meteorology and Climatology 46:1383–1395

Pleim JE (2007b) A combined local and nonlocal closure model for the atmospheric boundary layer. Part II: Application and evaluation in a mesoscale meteorological model. Journal of Applied Meteorology and Climatology 46:1396–1409

Pohl B, Crétat J, Camberlin P (2011) Testing WRF capability in simulating the atmospheric water cycle over Equatorial East Africa. Climate Dynamics 37:1357–1379, DOI 10.1007/s00382-011-1024-2

Pook MJ, Risbey JS, McIntosh PC (2011) The synoptic climatology of cool-season rainfall in the Central Wheatbelt of Western Australia. Monthly Weather Review 140:28–43, DOI 10.1175/MWR-D-11-00048.1

Prabha TV, Hoogenboom G, Smirnova TG (2011) Role of land surface parameterizations on modeling cold-pooling events and low-level jets. Atmospheric Research 99:147 – 161, DOI http://dx.doi.org/10.1016/j.atmosres.2010.09.017

Raupach MR, Briggs PR, Haverd V, King EA, Paget M, Trudinger CM (2008) Australian Water Availability Project. CSIRO Marine and Atmospheric Research, Canberra, Australia. http://www.csiro.au/awap. Accessed 22.10.2009

Raupach MR, Briggs PR, Haverd V, King EA, Paget M, Trudinger CM (2009) Australian Water Availability Project (AWAP): CSIRO Marine and Atmospheric Research Component: Final Report for Phase 3. CAWCR Technical Report No. 013. 67 pp.

Reason CJC, Gamble D, Pearce AF (1999) The leeuwin current in the parallel ocean climate model and applications to regional meteorology and fisheries. Meteorological Applications 6:211–225, DOI 10.1017/S1350482799001255

Reynolds RW, Smith TM (1994) Improved global sea surface temperature analyses using optimum interpolation. Journal of Climate 7:929–948

Reynolds RW, Rayner NA, Smith TM, Stokes DC, Wang W (2002) An improved in situ and satellite SST analysis for climate. Journal of Climate 15:1609–1625

Salathe E, Leung L, Qian Y, Zhang Y (2010) Regional climate model projections for the state of Washington. Climatic Change 102:51–75, 10.1007/s10584-010-9849-y

Schneider DP, Deser C, Fasullo J, Trenberth KE (2013) Climate data guide spurs discovery and understanding. Eos, Transactions American Geophysical Union 94:121–122, DOI 10.1002/2013EO130001

Skamarock WC, Klemp JB, Dudhia J, Gill DO, Barker DM, Duda MG, Huang XY, Wang W, Powers JG (2008) A description of the advanced research WRF version 3. NCAR Tech. Note NCAR/TN-475+STR, 113 pp., NCAR

Smirnova TG, Brown JM, Benjamin SG, Kim D (2000) Parameterization of cold-season processes in the maps land-surface scheme. Journal of Geophysical Research: Atmospheres 105(D3):4077–4086, DOI 10.1029/1999JD901047

Stéfanon M, Drobinski P, D'Andrea F, Lebeaupin-Brossier C, Bastin S (2013) Soil moisture-temperature feedbacks at meso-scale during summer heat waves over western Europe. Climate Dynamics pp 1–16, DOI 10.1007/s00382-013-1794-9

Tapp RG, Barrell SL (1984) The north-west Australian cloud band: Climatology, characteristics and factors associated with development. Journal of Climatology 4:411–424, DOI 10.1002/joc.3370040406

Taylor KE (2001) Summarizing multiple aspects of model performance in a single diagram. Journal of Geophysical Research 106:7183–7192, DOI 10.1029/2000JD900719

Yuan X, Liang XZ, Wood E (2012) WRF ensemble downscaling seasonal forecasts of China winter precipitation during 1982-2008. Climate Dynamics 39:2041–2058, DOI 10.1007/s00382-011-1241-8

Zhang Y, Dulière V, Mote PW, Salathé EP (2009) Evaluation of WRF and HadRM mesoscale climate simulations over the U.S. Pacific Northwest. Journal of Climate 22:5511–5526

Table 1: Summary of numerical experiments carried out (BC-boundary conditions, LSM-land surface model, LW-longwave radiation scheme, SW-shortwave radiation scheme, CS-cumulus scheme, PBL-planetary boundary layer scheme, SLS-surface layer scheme, SST-sea surface temperature source, MIC-microphysics scheme)

Experiment	BC	LSM	LW	SW	CS	PBL/SLC	SST	MIC
REF	NNRP	NOAH	RRTM	Dudhia	KF	YSU/MO	NNRP	WSM 5-class
N_SST	NNRP	NOAH	RRTM	Dudhia	KF	YSU/MO	NOAA	WSM 5-class
FNL	FNL	NOAH	RRTM	Dudhia	KF	YSU/MO	NCEP-FNL	WSM 5-class
ERA	ERA-INT	NOAH	RRTM	Dudhia	KF	YSU/MO	ERA-INT	WSM 5-class
RUC	NNRP	RUC	RRTM	Dudhia	KF	YSU/MO	NNRP	WSM 5-class
BMJ	NNRP	NOAH	RRTM	Dudhia	BMJ	YSU/MO	NNRP	WSM 5-class
RTG	NNRP	NOAH	RRTMG	RRTMG	KF	YSU/MO	NNRP	WSM 5-class
CAM	NNRP	NOAH	CAM	CAM	KF	YSU/MO	NNRP	WSM 5-class
AC2	NNRP	NOAH	RRTM	Dudhia	KF	AC2/MO	NNRP	WSM 5-class
AC2_P	NNRP	NOAH	RRTM	Dudhia	KF	AC2/PX	NNRP	WSM 5-class
3C	NNRP	NOAH	RRTM	Dudhia	KF	YSU/MO	NNRP	WSM 3-class
5C_D	NNRP	NOAH	RRTM	Dudhia	KF	YSU/MO	NNRP	WDM 5-class
FNL_RTG	FNL	NOAH	RRTMG	RRTMG	KF	YSU/MO	FNL	WSM 5-class
ERA_RTG	ERA-INT	NOAH	RRTMG	RRTMG	KF	YSU/MO	ERA-INT	WSM 5-class

Table 2: Seasonal absolute and percentage (shown in brackets) bias in maximum temperature (°C) for the experiments in Table 1, for the Costal (Coast), Agricultural (Agric), and Rangelands (Range) regions.

	DJF			MAM			JJA			SON		
	Coast	Agric	Range	Coast	Agric	Range	Coast	Agric	Range	Coast	Agric	Range
REF	-3.3	-3.9	-3.2	-0.7	-1.3	-1.8	-1.9	-1.9	-2.1	-3.0	-2.9	-1.7
	(-11%)	(-12%)	(-9%)	(-3%)	(-5%)	(-7%)	(-11%)	(-6%)	(-11%)	(-13%)	(-12%)	(-6%)
N_SST	-3.1	-3.7	-3.1	-0.8	-1.3	-1.5	-1.7	-1.8	-2.1	-3.0	-2.9	-1.6
	(-11%)	(-11%)	(-8%)	(-3%)	(-5%)	(-5%)	(-10%)	(-5%)	(-12%)	(-13%)	(-11%)	(-6%)
FNL	-0.7	-1.6	-1.9	0.1	-0.4	-0.7	-1.2	-1.6	-1.3	-1.5	-1.7	-1.1
	(-2%)	(-5%)	(-5%)	(0%)	(-2%)	(-3%)	(-7%)	(-5%)	(-7%)	(-7%)	(-7%)	(-4%)
ERA	-0.5	-1.2	-1.5	0.0	-0.5	-0.8	-1.3	-1.5	-1.3	-1.5	-1.5	-0.7
	(-2%)	(-4%)	(-4%)	(0%)	(-2%)	(-3%)	(-7%)	(-5%)	(-7%)	(-7%)	(-6%)	(-3%)
RUC	8.9	7.9	9.8	6.0	5.6	7.1	0.6	1.9	3.5	5.8	6.9	10.5
	(31%)	(24%)	(27%)	(26%)	(22%)	(26%)	(4%)	(6%)	(19%)	(26%)	(27%)	(40%)
BMJ	-3.2	-3.7	-3.1	-0.6	-1.0	-1.5	-1.8	-1.9	-2.3	-2.5	-2.6	-1.5
	(-11%)	(-11%)	(-9%)	(-3%)	(-4%)	(-6%)	(-11%)	(-6%)	(-12%)	(-11%)	(-10%)	(-5%)
RTG	-2.4	-3.0	-2.2	-0.2	-0.4	0.1	-0.7	-0.0	0.0	-2.1	-1.7	-0.4
	(-8%)	(-9%)	(-6%)	(-1%)	(-1%)	(0%)	(-4%)	(-0%)	(0%)	(-9%)	(-7%)	(-1%)
CAM	-3.0	-3.7	-2.9	-0.9	-1.3	-1.1	-1.7	-1.4	-1.6	-2.8	-2.5	-1.3
	(-11%)	(-11%)	(-8%)	(-4%)	(-5%)	(-4%)	(-10%)	(-4%)	(-9%)	(-12%)	(-10%)	(-5%)
AC2	-3.8	-4.6	-4.0	-0.5	-1.4	-2.2	-1.8	-1.9	-2.1	-3.7	-3.7	-2.5
	(-13%)	(-14%)	(-11%)	(-2%)	(-6%)	(-8%)	(-11%)	(-6%)	(-12%)	(-16%)	(-15%)	(-10%)
AC2_P	-1.3	-2.7	-2.0	0.6	-0.4	-1.0	-1.9	-1.7	-1.8	-2.7	-2.6	-1.1
	(-5%)	(-8%)	(-5%)	(3%)	(-1%)	(-3%)	(-11%)	(-5%)	(-9%)	(-12%)	(-10%)	(-4%)
3C	-3.2	-3.9	-3.3	-0.9	-1.4	-1.5	-1.7	-1.6	-2.1	-2.9	-2.8	-1.6
	(-11%)	(-12%)	(-9%)	(-4%)	(-5%)	(-6%)	(-10%)	(-5%)	(-11%)	(-13%)	(-11%)	(-6%)
5C_D	-3.0	-3.6	-3.0	-0.4	-0.9	-1.5	-1.5	-1.2	-1.4	-2.7	-2.6	-1.5
	(-10%)	(-11%)	(-8%)	(-2%)	(-4%)	(-5%)	(-9%)	(-4%)	(-7%)	(-12%)	(-10%)	(-6%)
FNL_RTG	0.3	-0.8	-1.5	1.0	0.5	-0.1	-0.1	-0.0	0.2	-0.4	-0.5	-0.1
	(1%)	(-2%)	(-4%)	(4%)	(2%)	(-0%)	(-0%)	(-0%)	(1%)	(-2%)	(-2%)	(-0%)
ERA_RTG	0.1	-0.8	-1.4	0.5	0.1	-0.6	-0.1	0.2	0.4	-0.5	-0.1	0.3
	(0%)	(-2%)	(-4%)	(2%)	(0%)	(-2%)	(-1%)	(1%)	(2%)	(-2%)	(-1%)	(1%)

Table 3: Same as in Table 2 except for minimum temperature (°C).

	DJF			MAM			JJA			SON		
	Coast	Agric	Range	Coast	Agric	Range	Coast	Agric	Range	Coast	Agric	Range
REF	-2.4	-1.8	-2.9	-1.4	-1.3	-2.9	-1.2	-2.2	-3.0	-1.5	-1.5	-1.9
	(-17%)	(-11%)	(-15%)	(-12%)	(-10%)	(-20%)	(-19%)	(-42%)	(-54%)	(-16%)	(-16%)	(-16%)
N_SST	-1.9	-1.2	-2.6	-1.1	-1.3	-3.0	-0.9	-2.2	-3.2	-1.1	-1.3	-1.7
	(-13%)	(-8%)	(-13%)	(-9%)	(-10%)	(-21%)	(-14%)	(-40%)	(-58%)	(-12%)	(-14%)	(-15%)
FNL	0.9	2.1	1.4	1.3	2.0	1.7	0.6	0.6	1.2	0.7	1.1	1.2
	(6%)	(13%)	(7%)	(11%)	(16%)	(12%)	(9%)	(11%)	(22%)	(7%)	(12%)	(10%)
ERA	0.6	1.9	1.3	1.0	1.8	1.8	0.5	0.7	1.3	0.8	1.2	1.5
	(4%)	(12%)	(6%)	(9%)	(15%)	(12%)	(9%)	(14%)	(23%)	(9%)	(13%)	(12%)
RUC	-1.4	-1.1	-1.6	-0.7	-1.2	-2.4	-0.5	-1.4	-2.9	-0.4	0.1	-0.5
	(-10%)	(-7%)	(-8%)	(-6%)	(-10%)	(-17%)	(-8%)	(-26%)	(-52%)	(-4%)	(1%)	(-4%)
BMJ	-2.4	-1.6	-2.9	-1.4	-1.4	-3.1	-1.1	-2.5	-3.5	-1.3	-1.4	-1.9
	(-17%)	(-10%)	(-14%)	(-12%)	(-11%)	(-22%)	(-18%)	(-47%)	(-63%)	(-14%)	(-15%)	(-16%)
RTG	-1.6	-0.9	-2.0	-0.7	-0.4	-1.3	-0.3	-0.5	-0.9	-0.9	-0.6	-0.6
	(-11%)	(-5%)	(-10%)	(-6%)	(-3%)	(-9%)	(-5%)	(-10%)	(-15%)	(-10%)	(-7%)	(-5%)
CAM	-2.8	-2.0	-3.2	-2.1	-2.0	-2.8	-2.2	-2.4	-3.0	-2.1	-1.7	-1.9
	(-20%)	(-12%)	(-16%)	(-18%)	(-16%)	(-20%)	(-35%)	(-45%)	(-54%)	(-23%)	(-18%)	(-16%)
AC2	-4.1	-3.5	-5.6	-2.7	-2.9	-5.3	-2.0	-2.8	-3.8	-3.1	-3.3	-4.3
	(-29%)	(-22%)	(-28%)	(-23%)	(-23%)	(-38%)	(-31%)	(-53%)	(-69%)	(-34%)	(-36%)	(-36%)
AC2_P	-5.1	-4.5	-6.4	-3.5	-3.7	-6.4	-3.0	-4.0	-5.4	-4.0	-4.2	-5.6
	(-36%)	(-28%)	(-32%)	(-30%)	(-30%)	(-45%)	(-47%)	(-75%)	(-97%)	(-43%)	(-45%)	(-48%)
3C	-2.4	-1.7	-3.1	-1.6	-1.6	-2.9	-1.3	-2.2	-3.1	-1.5	-1.6	-1.9
	(-16%)	(-11%)	(-15%)	(-14%)	(-13%)	(-21%)	(-20%)	(-41%)	(-56%)	(-16%)	(-17%)	(-16%)
5C_D	-2.3	-1.7	-2.8	-1.1	-0.9	-2.6	-0.8	-1.7	-2.4	-1.4	-1.3	-1.7
	(-16%)	(-11%)	(-14%)	(-9%)	(-8%)	(-19%)	(-12%)	(-32%)	(-43%)	(-15%)	(-14%)	(-15%)
FNL_RTG	1.3	2.6	1.9	1.8	2.8	2.6	1.4	1.9	2.8	1.4	2.1	2.4
	(9%)	(16%)	(9%)	(16%)	(23%)	(19%)	(23%)	(35%)	(50%)	(15%)	(23%)	(20%)
ERA_RTG	1.1	2.5	1.8	1.6	2.6	2.5	1.4	1.9	2.9	1.5	2.2	2.5
	(7%)	(15%)	(9%)	(14%)	(21%)	(18%)	(22%)	(36%)	(52%)	(16%)	(24%)	(21%)

Table 4: Same as in Table 2 except for precipitation (mm month^{-1}).

	DJF			MAM			JJA			SON		
	Coast	Agric	Range	Coast	Agric	Range	Coast	Agric	Range	Coast	Agric	Range
REF	4.1	-0.1	-8.4	-18.9	-20.0	-18.3	-13.3	-21.4	-15.4	-6.9	-4.1	-13.2
	(117%)	(-1%)	(-87%)	(-38%)	(-68%)	(-82%)	(-14%)	(-55%)	(-83%)	(-20%)	(-34%)	(-91%)
N_SST	5.3	1.1	-8.4	-16.5	-19.8	-19.7	-3.8	-18.1	-15.5	-2.0	-3.2	-13.0
	(150%)	(20%)	(-87%)	(-33%)	(-67%)	(-89%)	(-4%)	(-46%)	(-83%)	(-6%)	(-26%)	(-89%)
FNL	7.2	7.3	9.5	-16.1	-7.9	5.8	12.6	3.5	6.0	-0.9	3.2	-4.2
	(206%)	(141%)	(99%)	(-32%)	(-27%)	(26%)	(14%)	(9%)	(32%)	(-2%)	(27%)	(-29%)
ERA	2.2	2.6	8.9	-9.9	-4.1	9.6	6.8	-0.7	4.1	3.8	2.3	-4.3
	(62%)	(49%)	(92%)	(-20%)	(-14%)	(44%)	(7%)	(-2%)	(22%)	(11%)	(19%)	(-30%)
RUC	4.6	-0.3	-8.3	-22.7	-21.7	-19.6	-19.1	-20.1	-13.9	-9.4	-5.0	-13.1
	(132%)	(-7%)	(-86%)	(-45%)	(-74%)	(-89%)	(-20%)	(-51%)	(-74%)	(-27%)	(-41%)	(-91%)
BMJ	2.7	-1.8	-8.8	-26.9	-23.9	-20.4	-24.4	-21.2	-15.1	-14.4	-6.2	-13.7
	(75%)	(-34%)	(-91%)	(-54%)	(-81%)	(-92%)	(-26%)	(-54%)	(-81%)	(-42%)	(-51%)	(-95%)
RTG	4.1	-0.3	-8.6	-21.4	-19.0	-19.5	-21.0	-20.5	-15.5	-12.2	-6.3	-13.3
	(116%)	(-5%)	(-89%)	(-43%)	(-64%)	(-88%)	(-23%)	(-52%)	(-83%)	(-35%)	(-52%)	(-92%)
CAM	3.2	-0.1	-8.5	-19.4	-20.0	-17.7	-17.4	-19.7	-15.2	-12.5	-5.2	-12.9
	(90%)	(-2%)	(-88%)	(-39%)	(-68%)	(-80%)	(-19%)	(-50%)	(-82%)	(-36%)	(-43%)	(-89%)
AC2	4.6	-0.4	-7.8	-20.9	-21.9	-19.4	-6.2	-17.4	-14.9	-6.1	-3.1	-12.6
	(131%)	(-8%)	(-80%)	(-42%)	(-74%)	(-88%)	(-7%)	(-44%)	(-80%)	(-18%)	(-25%)	(-87%)
AC2_P	3.4	-0.4	-8.5	-16.1	-21.5	-19.5	-3.2	-14.5	-14.3	-4.1	-2.5	-12.9
	(98%)	(-7%)	(-88%)	(-32%)	(-73%)	(-88%)	(-3%)	(-37%)	(-76%)	(-12%)	(-21%)	(-89%)
3C	3.7	0.5	-8.3	-20.0	-21.4	-19.0	-17.0	-21.7	-15.6	-7.8	-4.7	-13.2
	(105%)	(10%)	(-86%)	(-40%)	(-72%)	(-86%)	(-18%)	(-55%)	(-84%)	(-23%)	(-39%)	(-91%)
5C_D	5.7	0.2	-8.2	-15.0	-17.8	-18.9	-8.9	-19.1	-14.8	-5.5	-3.1	-13.0
	(163%)	(3%)	(-84%)	(-30%)	(-60%)	(-86%)	(-10%)	(-49%)	(-79%)	(-16%)	(-25%)	(-89%)
FNL_RTG	5.6	7.6	22.3	-19.3	-3.5	19.0	4.2	8.3	10.0	-2.9	4.6	1.2
	(160%)	(146%)	(230%)	(-39%)	(-12%)	(86%)	(5%)	(21%)	(53%)	(-8%)	(38%)	(8%)
ERA_RTG	3.7	7.5	21.3	-10.8	3.5	25.3	-0.9	-2.6	3.6	-4.5	2.4	2.9
	(106%)	(145%)	(220%)	(-22%)	(12%)	(114%)	(-1%)	(-7%)	(19%)	(-13%)	(20%)	(20%)

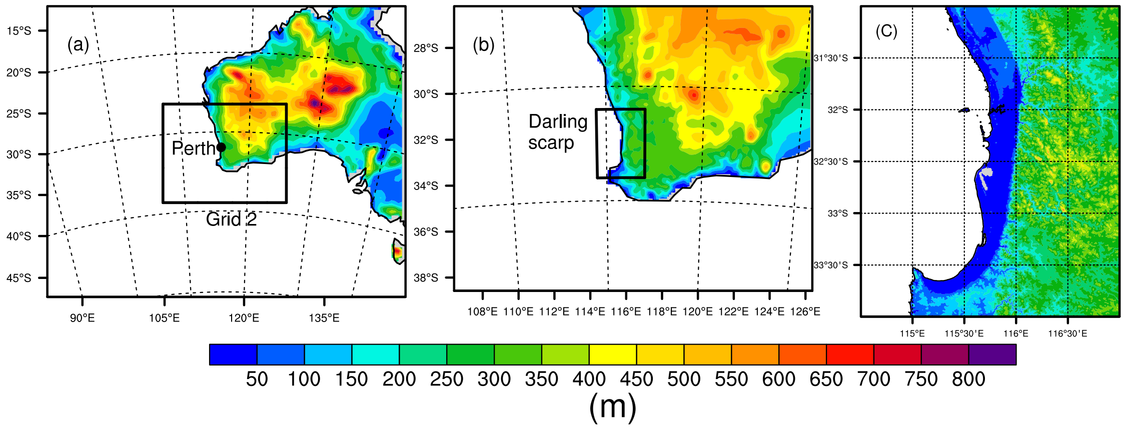

Fig. 1: (a) Map showing the topography of the outer grid domain (50-km resolution), the boundary of the second inner nested grid representing SWWA, and the location of the city of Perth; (b) topography of the second inner nested domain (10-km resolution) and location of the Darling scarp, and; (c), topography of the Darling scarp (9-arc seconds topography from Geoscience Australia (Hutchinson et al, 2009)). Note that the maps shown in (a) and (b) are the computational grids used for the simulations whereas the map shown in (c) is only for the purpose of illustrating the sharp increase in topography associated with the Darling scarp.

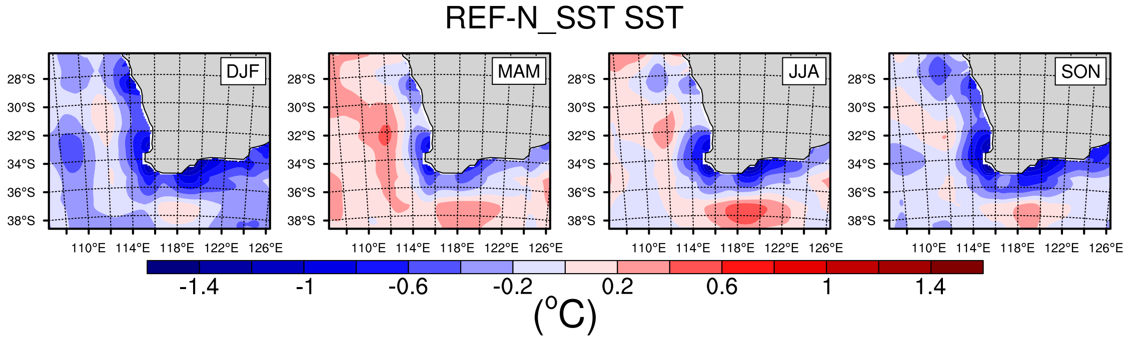

Fig. 2: Countour plots showing the difference in sea surface temperature between the REF and N_SST experiments (C) by season. Negative values indicate that the N_SST simulation had higher sea surface temperatures relative to REF.

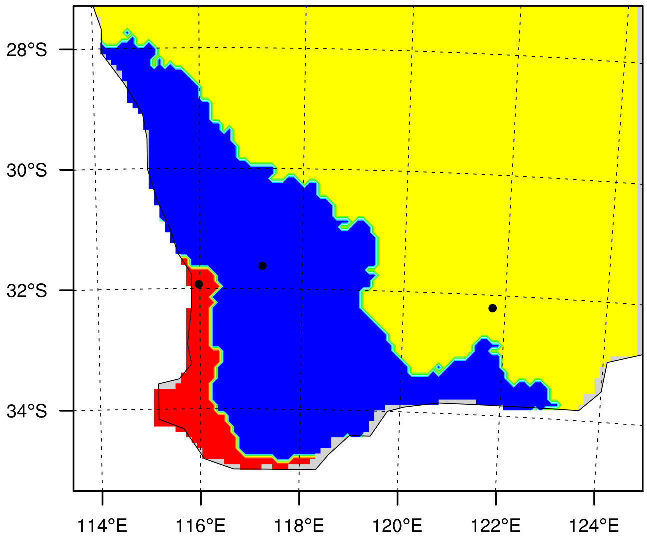

Fig. 3: Regionalisation used during analysis (red = coast, blue = agricultural region, yellow = rangelands). Each black dot in the 3 regions represent the location of a precipitation station used for further analysis, namely, the Perth Airport station at the coast, the Cunderdin in the agricultural region, and Norseman in the rangelands.

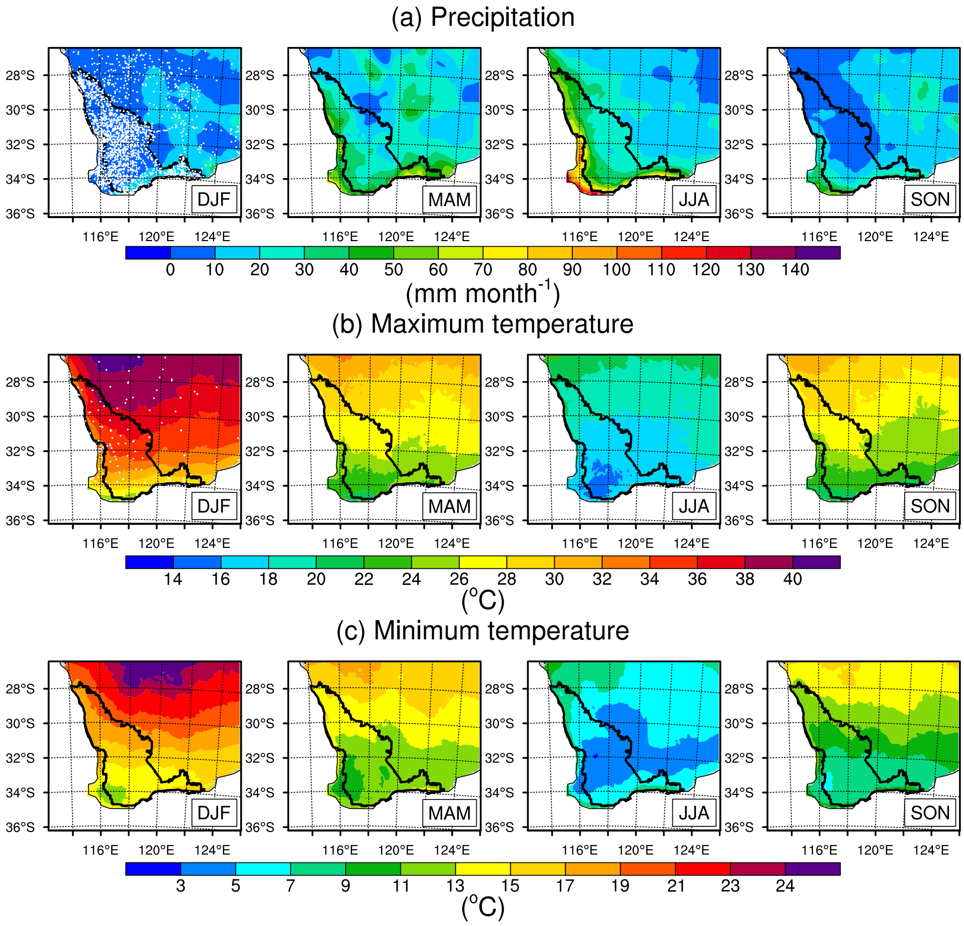

Fig. 4: (a) Precipitation (mm month^{-1}), (b) maximum temperature (°C), and (c) minimum temperature over SWWA during DJF, MAM, JJA, and SON of 2010 from the Australian Bureau of Meteorology. White dots in the DJF panels (a) and (b) show precipitation and temperature station locations and the black solid line represents the approximate boundaries of the agricultural region.

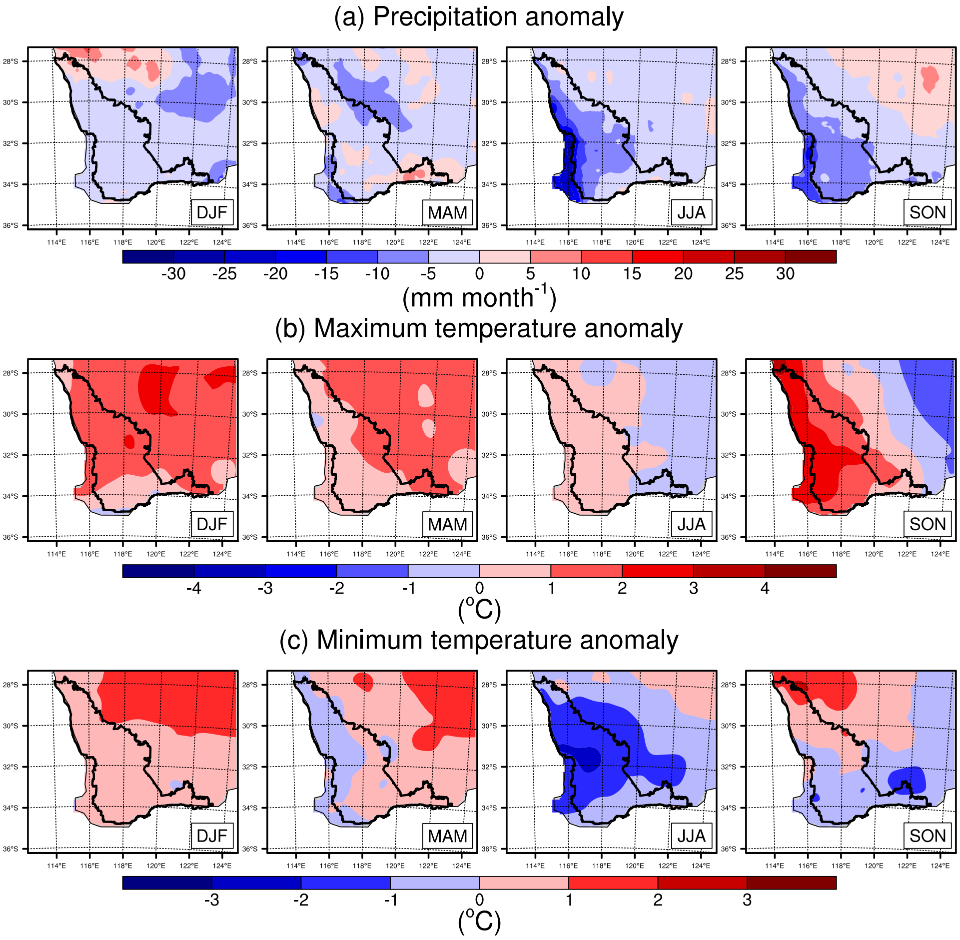

Fig. 5: Same as in Fig. 4 except showing the seasonal 2010 anomaly from 1970-2010.

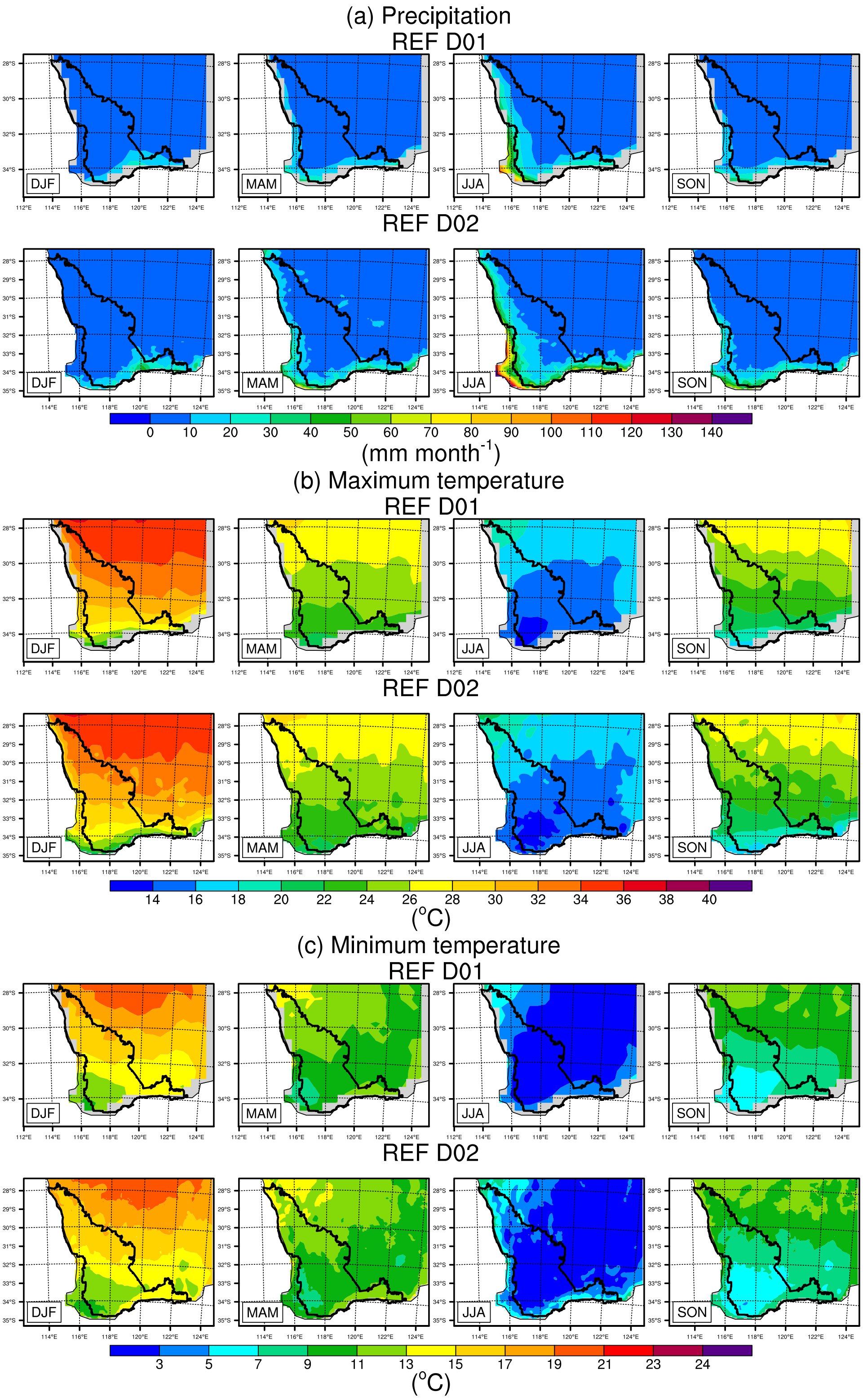

Fig. 6: (a) Precipitation (mm month^{-1}), (b) maximum temperature (°C), and (c) minimum temperature over SWWA during DJF, MAM, JJA, and SON of 2010 from the outer 50-km domain (D01) and inner 10-km nested domain (D02) for the REF experiment (Table 1).

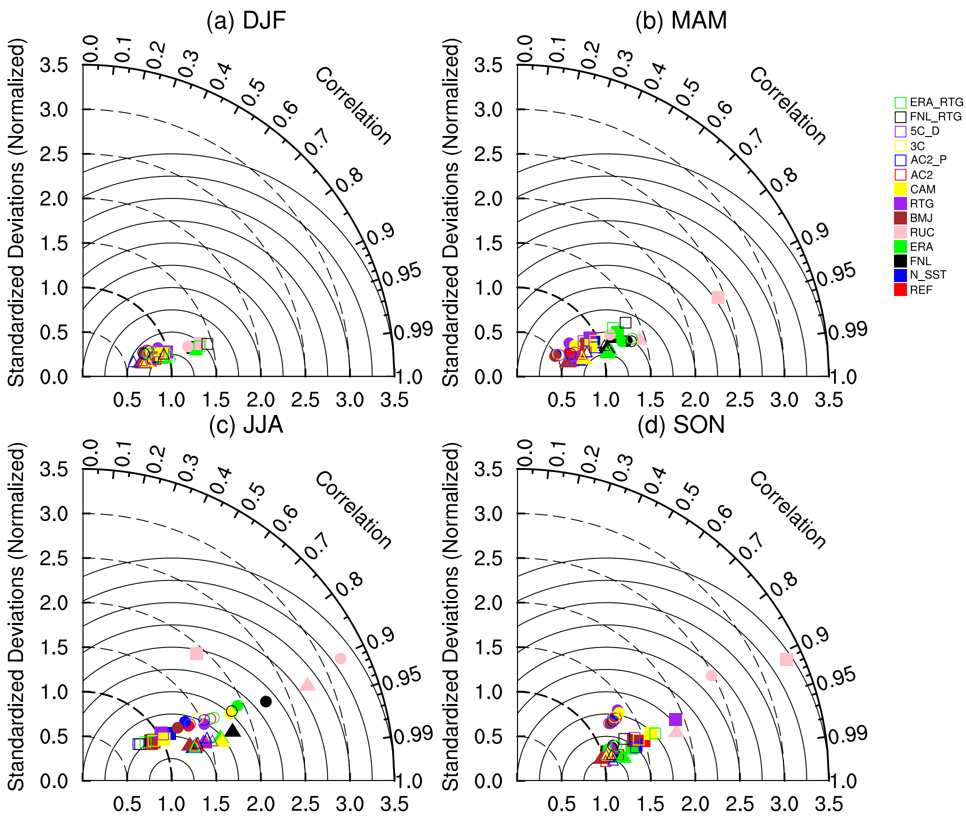

Fig. 7: Taylor diagrams for maximum temperature during (a) DJF, (b) MAM, (c) JJA, and (d) SON, for the experiments in Table 1, for the coastal region (squares), the agricultural region (triangles), and rangelands (circles).

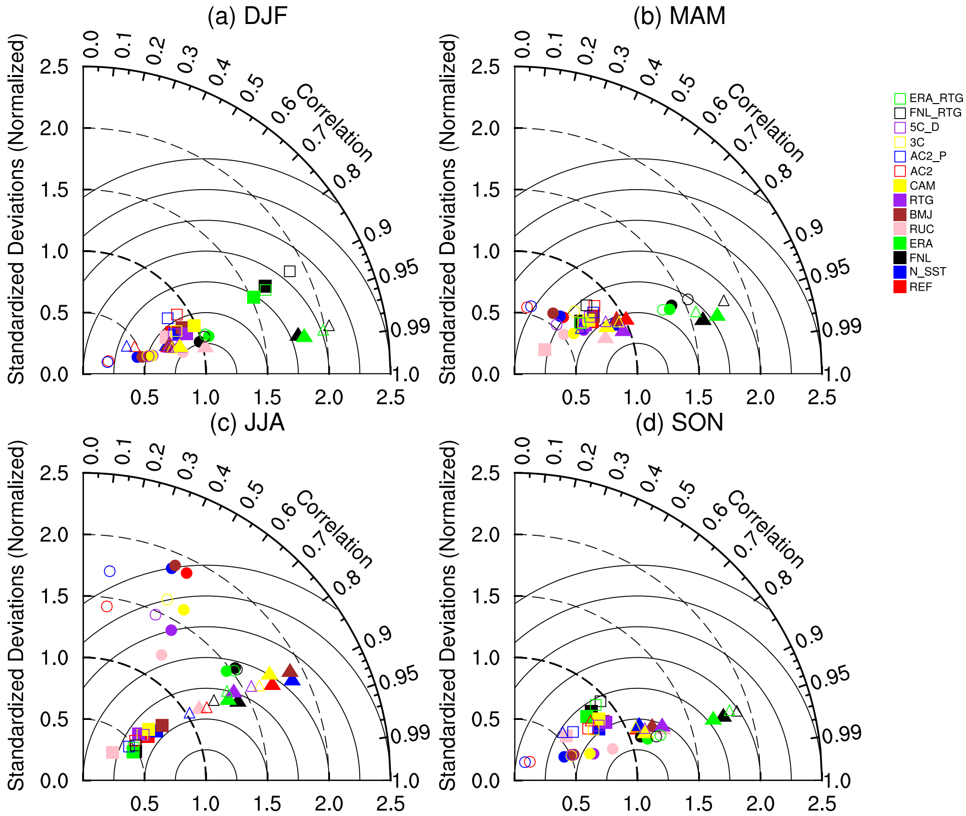

Fig. 8: Same as in Figure 7, except for minimum temperature.

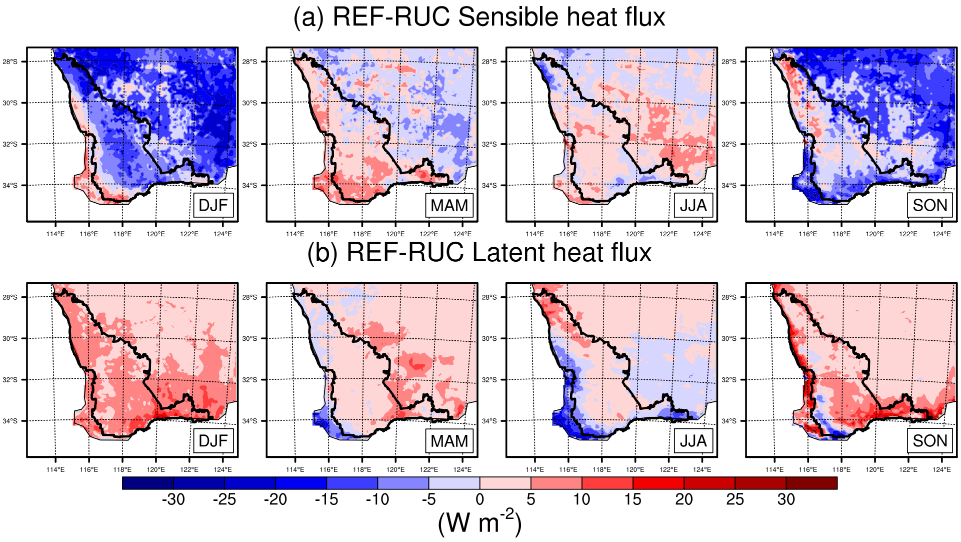

Fig. 9: Differences in seasonal (a) sensible, and (b) latent heat flux (W m^{-2}) between the REF and RUC experiments (Table 1)

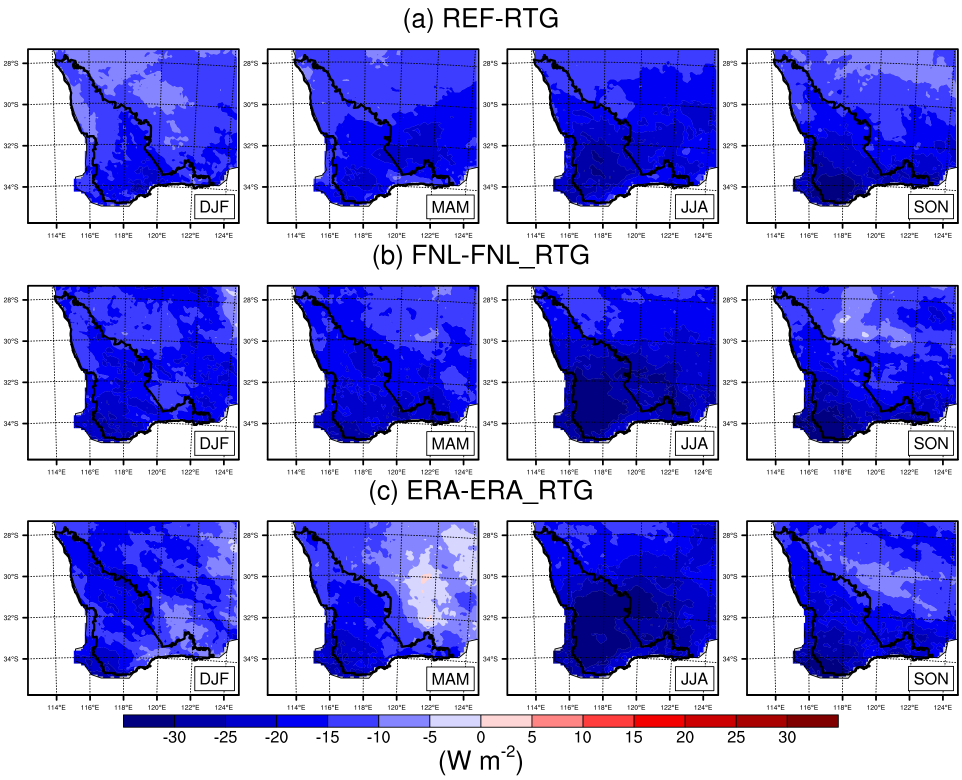

Fig. 10: Seasonal means of differences in incoming shortwave radiation (W m^{-2}) between the (a) REF and RTG, (b) FNL and FNL_RTG, and (c) ERA and ERA_RTG experiments (Table 1).

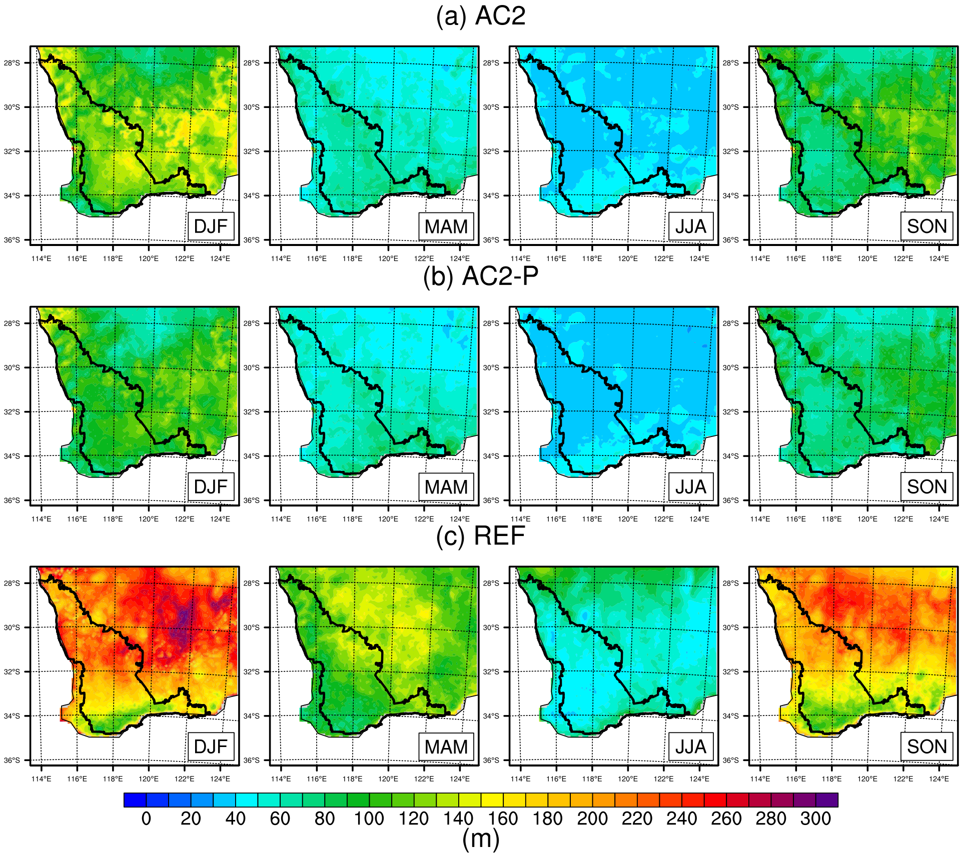

Fig. 11: Seasonal means of minimum PBL heights for (a) AC, (b) AC2_P, and (c) REF simulations (Table 1).

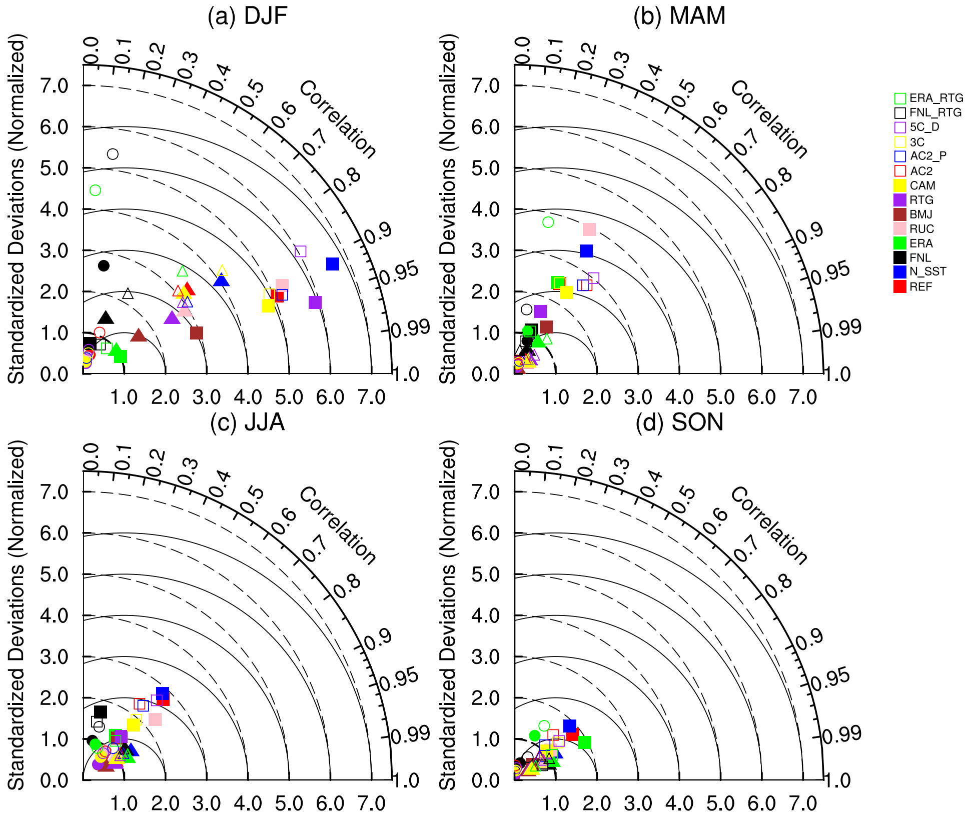

Fig. 12: Same as in Figure 7, except for precipitation.

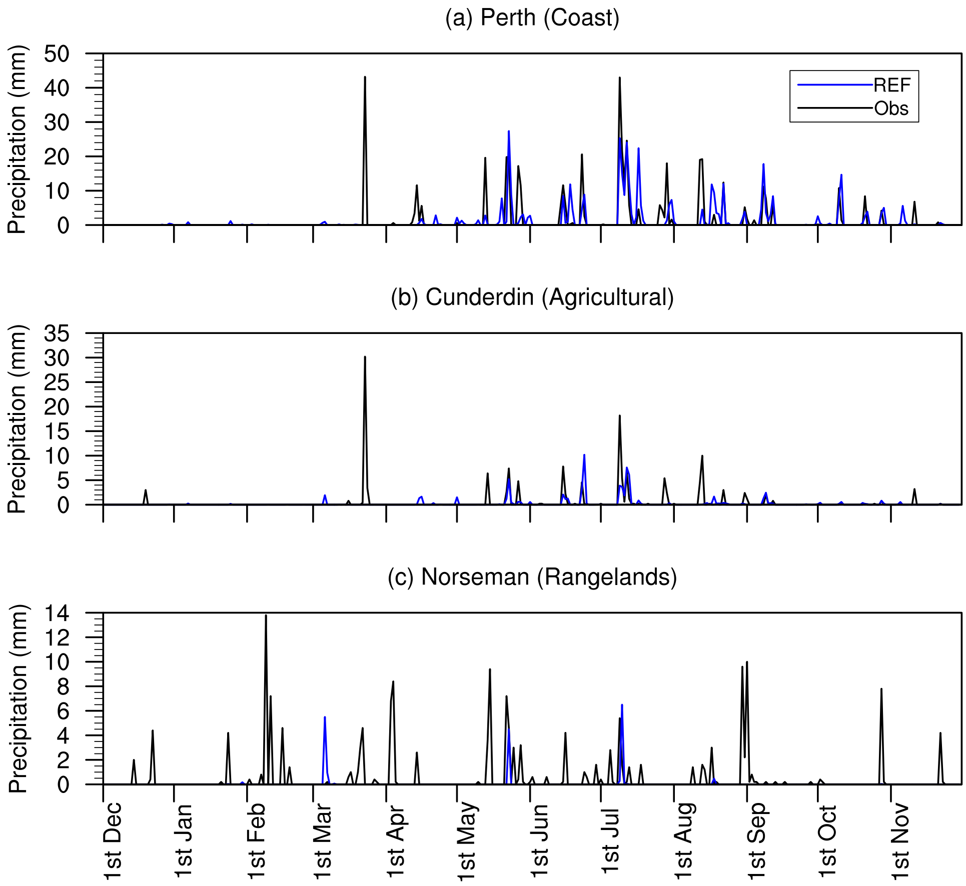

Fig. 13: Time series of daily precipitation (mm) from 1st of December 2009 to 30th of November 2010 at the: (a) Perth (Coast), (b) Cunderdin (Agricultural), and (c) Norseman (Rangelands) stations (Fig. 3). Black lines represent the observations and the blue lines the REF experiment.

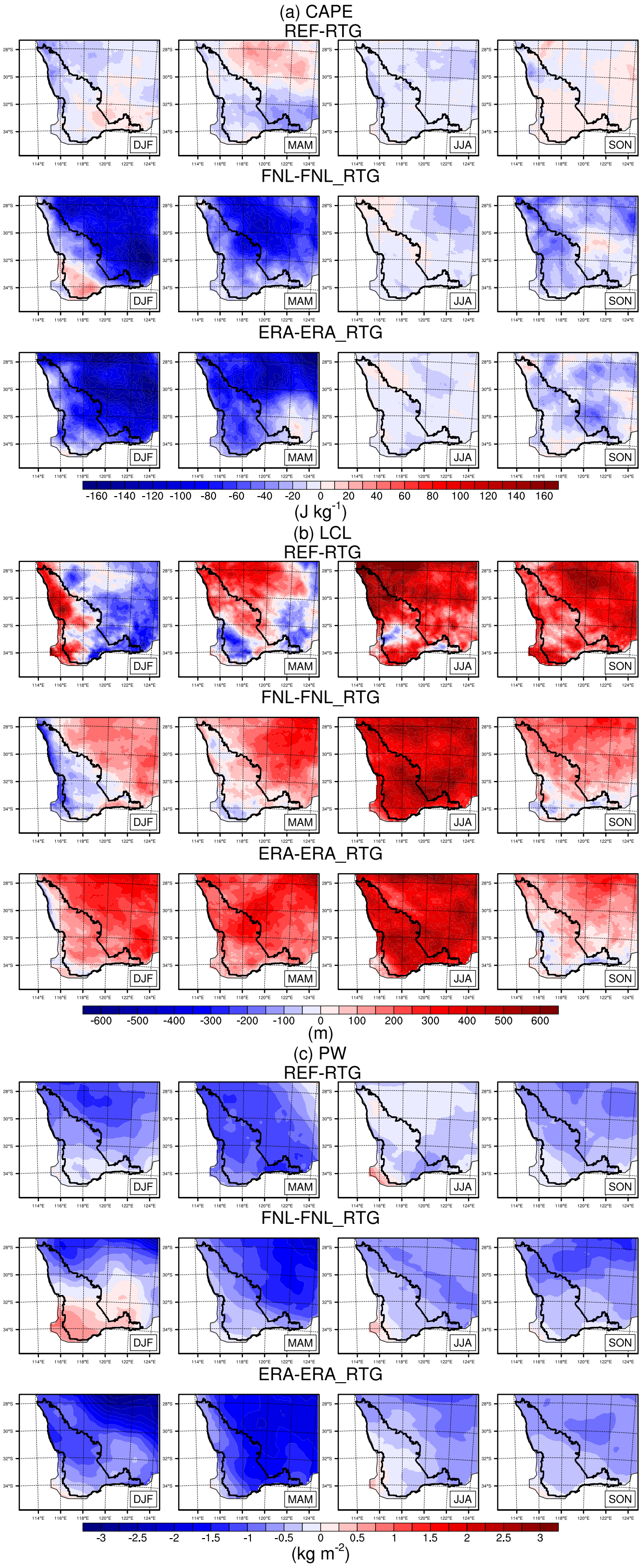

Fig. 14 Differences in: (a) Convective Available Potential Energy (CAPE) (J kg^{-1}), (b) Lifting Condensation Level (LCL) (m), and (c) Precipitable Water (PW) (kg m^{-2}) between the REF and RTG (REF-RTG), FNL and FNL_RTG (FNL - FNL_RTG), and ERA and ERA_RTG (ERA - ERA_RTG) experiments (Table 1).